AD_____

Award Number: DAMD17-03-1-0755

TITLE: Therapy of Ovarian Carcinoma by Targeted Delivery of Alpha-Particles Using Immunoliposomes Capable of Retaining Alpha-Emitting Daughters

PRINCIPAL INVESTIGATOR:George Sgouros, Ph.D.

CONTRACTING ORGANIZATION: Johns Hopkins University
School of Medicine
Baltimore, MD 21205

REPORT DATE: October 2005

TYPE OF REPORT: Annual

PREPARED FOR: U.S. Army Medical Research and Materiel Command
Fort Detrick, Maryland 21702-5012

DISTRIBUTION STATEMENT:

X Approved for public release; distribution unlimited

☐ Distribution limited to U.S. Government agencies only; report contains proprietary information

The views, opinions and/or findings contained in this report are those of the author(s) and should not be construed as an official Department of the Army position, policy or decision unless so designated by other documentation.

REPORT DOCUMENTATION PAGE

Form Approved
OMB No. 0704-0188

Public reporting burden for this collection of information is estimated to average 1 hour per response, including the time for reviewing instructions, searching existing data sources, gathering and maintaining the data needed, and completing and reviewing this collection of information. Send comments regarding this burden estimate or any other aspect of this collection of information, including suggestions for reducing this burden to Department of Defense, Washington Headquarters Services, Directorate for Information Operations and Reports (0704-0188), 1215 Jefferson Davis Highway, Suite 1204, Arlington, VA 22202-4302. Respondents should be aware that notwithstanding any other provision of law, no person shall be subject to any penalty for failing to comply with a collection of information if it does not display a currently valid OMB control number. **PLEASE DO NOT RETURN YOUR FORM TO THE ABOVE ADDRESS.**

1. REPORT DATE	2. REPORT TYPE	3. DATES COVERED
01-10-2005	Annual	30 Sep 2004 – 29 Sep 2005

4. TITLE AND SUBTITLE

Therapy of Ovarian Carcinoma by Targeted Delivery of Alpha-Particles Using Immunoliposomes Capable of Retaining Alpha-Emitting Daughters

5a. CONTRACT NUMBER

5b. GRANT NUMBER
DAMD17-03-1-0755

5c. PROGRAM ELEMENT NUMBER

6. AUTHOR(S)

George Sgouros, Ph.D.

5d. PROJECT NUMBER

5e. TASK NUMBER

5f. WORK UNIT NUMBER

7. PERFORMING ORGANIZATION NAME(S) AND ADDRESS(ES)

Johns Hopkins University
School of Medicine
Baltimore, MD 21205

8. PERFORMING ORGANIZATION REPORT NUMBER

9. SPONSORING / MONITORING AGENCY NAME(S) AND ADDRESS(ES)
U.S. Army Medical Research and Materiel Command
Fort Detrick, Maryland 21702-5012

10. SPONSOR/MONITOR'S ACRONYM(S)

11. SPONSOR/MONITOR'S REPORT NUMBER(S)

12. DISTRIBUTION / AVAILABILITY STATEMENT
Approved for Public Release; Distribution Unlimited

13. SUPPLEMENTARY NOTES
Original contains colored plates: ALL DTIC reproductions will be in black and white.

14. ABSTRACT The objective of this work is to develop a liposomal system for encapsulating alpha-particle emitting radionuclides for use in IP-administered targeted therapy of ovarian cancer metastases. The scope of the overall project includes development, stability, and radionuclide retention testing of the liposomes as well as the evaluation of their targeting properties, in vitro, and in vivo (aims 1 and 2). This is to be followed by evaluation of tumor cell kill using monolayer cell culture, spheroid culture and in tumor-bearing animals (aims 3 and 4). In the first progress report, completion of Task 1 and the majority of Task 2 was reported. Although retention of the parent, 225Ac was 88%, retention of 213Bi, the last daughter in the decay chain was only 4 to 5% after 30 days (JNM '04). The previous report ended with a brief description of a novel liposomal construct (multi-vesicular liposome – MUVEL) that had been engineered to address the known reasons for low 213Bi retention. Over the past year, this new construct has been characterized, both, in vitro and in vivo. Although not as large as expected theoretically, the MUVEL structures increased 213Bi retention from 5% to 18%. Animal studies demonstrated tumor to kidney ratios that were comparable to Ac-225-labeled antibody, however. Preloading of liposomes to reduce RES uptake will be investigated improve this ratio as the work moves to efficacy and toxicity studies in year 3.

15. SUBJECT TERMS
Radioimmunotherapy, alpha-particle, immunoliposome, HER2/neu, Ac-225

16. SECURITY CLASSIFICATION OF:				18. NUMBER OF PAGES	19a. NAME OF RESPONSIBLE PERSON
					USAMRMC
a. REPORT	b. ABSTRACT	c. THIS PAGE			19b. TELEPHONE NUMBER *(include area code)*
U	U	U	UU	107	

Standard Form 298 (Rev. 8-98)
Prescribed by ANSI Std. Z39.18

Table of Contents

Cover……

SF 298……

Table of Contents……2

Introduction……3

Body……3

Key Research Accomplishments……11

Reportable Outcomes……11

Conclusions……12

References……12

Appendices……14

Annual Report - Therapy of Ovarian Carcinoma by Targeted Delivery of Alpha-Particles Using Immunoliposomes Capable of Retaining Alpha-Emitting Daughters

INTRODUCTION

Disseminated, metastatic ovarian carcinoma is largely incurable. This project is intended to develop and evaluate targeted, alpha-particle emitter loaded liposomes –alpha radioimmunoliposomes (ARILs)- for therapy of IP-disseminated ovarian cancer metastases. Through previous DOD funding we examined the feasibility of liposomal encapsulation of the potent alpha-particle emitter actinium-225 in order to retain daughter emissions at the targeted site. In this grant we proposed to coat the liposomes with anti-HER2/neu antibodies, test their stability and tumor targeting characteristics, *in vitro* and *in vivo*. The tumor cell killing potential of ARILs as well as their normal organ toxicity will also be evaluated by a combination of studies performed, *in vitro* and *in vivo*.

In the first progress report, completion of Task 1 (to develop and characterize large immunoliposomes) and the majority of Task 2 (load the liposomes with ^{225}Ac and characterize daughter retention under different conditions) was reported. Although retention of the parent, ^{225}Ac was 88%, retention of ^{213}Bi, the last daughter in the decay chain was only 4 to 5% after 30 days (JNM '04). The previous report ended with a brief description of a novel liposomal construct (multi-vesicular liposome – MUVEL) that had been engineered to address the known reasons for low ^{213}Bi retention. Over the past year, this new construct has been characterized, both, *in vitro* and *in vivo*. This report focuses on these results.

BODY

Tasks 1 and 2 were repeated for the MUVEL structures first described in the previous report. Results are briefly summarized in the body of this report. The Appendix includes a manuscript that will soon be submitted to Cancer Research and that describes the MUVEL system in detail.

The low retention of ^{213}Bi using 700 to 800 nm diameter has led to the development of a novel liposomal construct – MUVEL for multi-vesicular liposome. A brief description of these is provided below. These constructs are made up of small (100 nm-diameter) unilamelar vesicles within which the ^{225}Ac is encapsulated. These are, in turn, encapsulated into larger (600-700 nm-diameter) liposomes. This approach provides a greater lipid content to which the daughters elements may bind, thereby reducing binding to the inner surface of the larger liposome which would reduce retention of the daughter elements. The figure above, on the left, depicts an electron micrograph showing the structure of the envisioned construct (on the right).

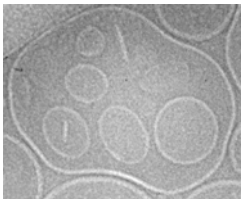

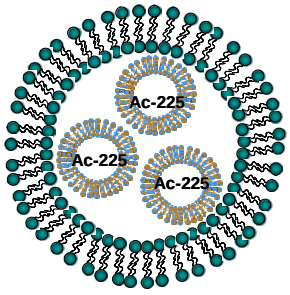

Liposome Characterization

Liposome size distributions were determined by DLS. The measured average large liposome size for MUVELs was 758 ± 287 nm. The phospholipid-cholesterol combinations chosen for the small encapsulated vesicles and the large liposome shells were those that resulted in: (1) the lowest release of contents by the small vesicles after annealing at 40^{o}C (this step is required for the hydration of the membranes of the large shell liposomes that contain encapsulated small vesicles), (2) the greatest passive entrapment efficacy, of total activity used, by the large liposome shells, and (3) the minimum fraction of fusion between lipids of small vesicles and large liposomes. Stability of the various membrane structures over time was evaluated by entrapment of a fluorophore (calcein) and assessment of content retention. Content retention by all structures was high for a period of 30 days (data not shown).

Retention of ^{225}Ac by the Liposomal Structures

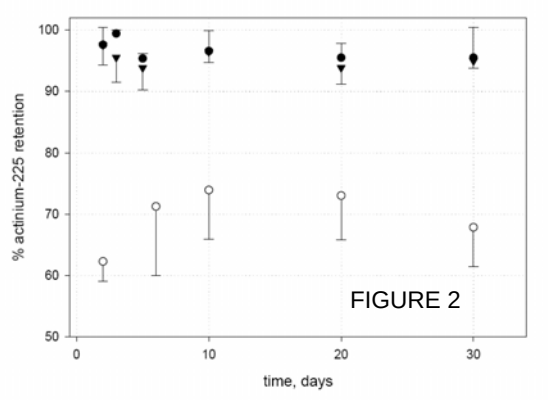

For 30 days, more than 95% of the encapsulated ^{225}Ac activity was retained by the multivesicular liposomes (black triangles) and small vesicles (black circles) (Figure 2 of manuscript). The large shell liposomes with encapsulated ^{225}Ac directly within their aqueous compartment retained stably only about 70% of the total activity (white circles) (Figure 2)

Retention of ^{213}Bi by the Liposomal Structures

Retention of ^{213}Bi, the last α-emitting daughter of ^{225}Ac, was then evaluated (Figure 3).

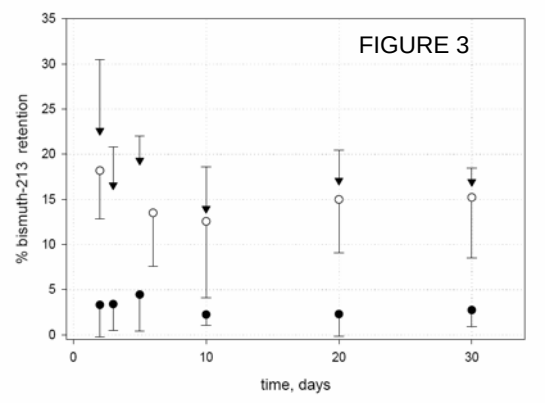

Multivesicular liposomes (black triangles) and large shell liposomes (white circles) stably retained approximately 18% of ^{213}Bi (32% of the theoretical maximum)(13). Both large liposome structures exhibited almost identical ^{213}Bi retention profiles suggesting that the particular composition of the (external) liposomal membrane does not promote radionuclide localization as opposed to the lipid composition chosen in our first studies (13). However, as shown above (Figure 2), large shell liposomes failed to adequately retain the parent ^{225}Ac. Also, consistent with our previous theoretical predictions, is the significantly low extent of ^{213}Bi retention (black circles) by small vesicles which have sizes comparable to the recoil range of the α-emitting daughters (28).

Liposome and Antibody Radiolabeling and Quality Control

More than 95% of ^{225}Ac was chelated to the DOTA derivative. The efficiency of conjugation to antibody was low with radiochemical yield 3% (of the total activity applied) and resulted in radiolabeled antibodies with low specific activity, 0.038 μCi/μg.

The maximum encapsulation efficiency of ^{225}Ac by the liposomal structures using passive entrapment did not exceed 10% of the total initial activity, and resulted in one ^{225}Ac nuclide in approximately every eight-to-nine MUVELs.

Immunoreactivity is expressed as per construct and per Trastuzumab molecule. The Her2/neu cell-surface density of 1-3 x 10^5 for these cells was used (29), and approximately one hundred Trastuzumab molecules per cell were mixed. For liposomal structures, two ratios were tested: (a) one hundred liposomes per cell, and (b) one liposome per cell (assuming an estimate of 100 conjugated Trastuzumab antibodies per liposome). The antigen binding activity of liposomes was similar for both ratios tested: 4.40 ± 0.89 % of immunolabeled multivesicular liposomes, and 1.83 ± 0.52 % of immunolabeled large shells were bound to cells. Small plain vesicles bound non-specifically at the extent of 0.75 ± 0.02 %. The immunoreactivity of radiolabeled Trastuzumab was 65.74 ± 7.51 %.

Liposome immunolabelling

The conjugation reaction resulted in 100-500 antibodies per liposome. Leakage of entrapped radioactive or fluorescent (calcein) contents due to conjugation, was not detected (data not shown).

Cell Binding and Internalization

To quantitatively determine binding, and intracellular retention of liposomal contents, all liposomal structures with entrapped ^{225}Ac, and also the radiolabeled antibody, were incubated at 37°C with SKOV3 cell suspensions for different times. Figure 4 shows the fraction of the total initial-activity that became cell-associated (closed symbols), and the fraction of cell-internalized activity (open symbols) for all cell-bound structures. All structures exhibited increase in cell-associated radioactivity with time, followed by gradual saturation of receptor internalization. The total cell-associated radioactivity at different times after start of incubation was compared to that immediately after the start of incubation (t=0). After 4 hours, the relative increases were a 2-, 7- and 135-fold for large shell immunoliposomes (squares), MUVELs (circles), and radiolabeled antibody (triangles), respectively. At 4 hours, the fraction of total cell-associated activity for non-immunolabeled MUVELS, large shells and small vesicles was 0.47%, 0.61% and 0.16% of the total added radioactivity, respectively (data not shown). After 4 h of incubation, the fraction of total cell-associated activity (^{225}Ac) delivered by specifically targeted multivesicular immunoliposomes (2.5 ± 0.5 %) was 3.8 times greater than the fraction of total associated

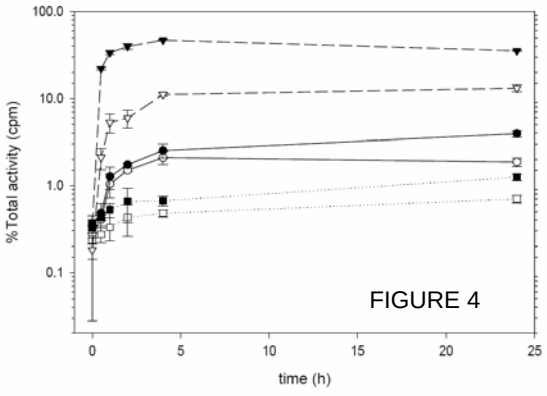

FIGURE 4

radioactivity delivered by large shell immunoliposomes (0.7 ± 0.1 %), probably due to the less stable retention of the parent nuclide by the large shell liposomes (Figure 2). Also, immunoliposomes internalized to a greater extent than the antibody: 83% of the activity of bound multivesicular immunoliposomes, and 70% of the activity of large shell immunoliposomes were internalized (4 h incubation) as opposed to only 23% of bound antibody. Cell uptake kinetics were significantly slower for all liposome structures compared to the radiolabeled antibody.

Flow cytometry was also used to evaluate the specific binding of immunoliposomes (by monitoring the fluorescently labeled membranes) to cell suspensions expressing, or not, the HER2/neu receptor (SKOV3 and AL67 fibroblast cell lines, respectively) (Figure 5). Significant shift in fluorescence counts (one log unit) that signifies enhanced binding of liposomes to cells was detected only when immunoliposomes were incubated with SKOV3 cells with unblocked HER2/neu receptors (Figure 5A, thick line). Neither specific nor non-specific binding of liposomes to AL67 cells was detected.

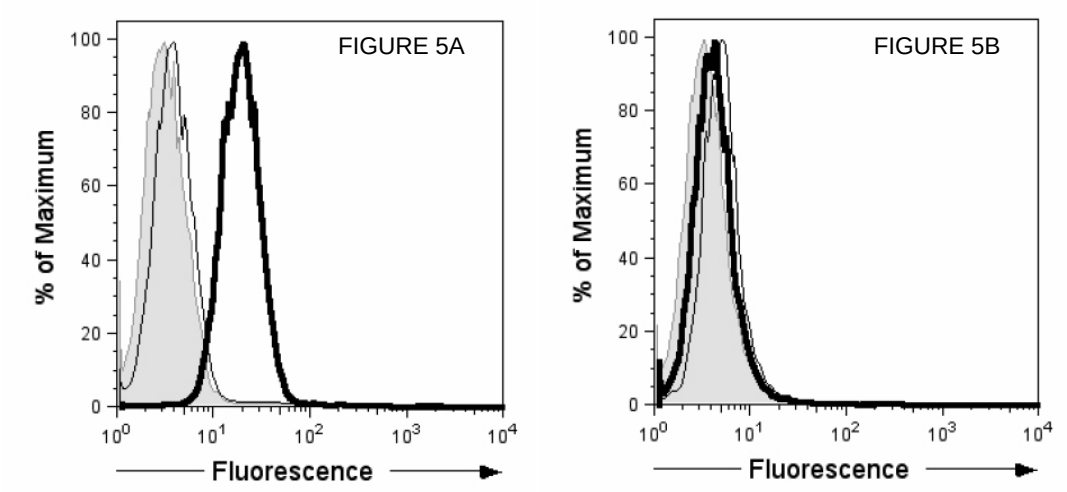

Whole body retention by tumor free mice

The whole body clearance of ^{221}Fr and ^{213}Bi in tumor free mice was low when radionuclides were administered within liposomal structures. Twenty-four hours post-administration, at least 81 % of the initial whole body activity was retained. On the contrary, rapid whole body clearance was observed after administration of ^{225}Ac-DOTA: Four hours post injection more than 90% of the total injected activity of ^{213}Bi and more than 96 % of ^{221}Fr was cleared from the body. No preferential clearance between the two radioactive daughters was observed when liposomes were used. At all time points, the ratios of the activity of ^{221}Fr to the activity of ^{213}Bi did not significantly deviate from the value obtained for the glass vial 'phantom' that contained the radioisotopes at equilibrium conditions.

Biodistributions of Liposomal Structures in Tumor Bearing Mice

Biodistributions of all liposomal structures and the free radiolabeled antibody were determined in tumor bearing mice. Fourteen days after inoculation, a tumor pattern was formed, that consisted of nodules on the ventral side of the spleen. Smaller nodules (~ 1mm in diameter) were frequently observed within the mesentery. The mean weight of removable tumor nodules was 0.3 ± 0.2 g (n=29, total number of animals). The normal organ accumulation of liposomes reached steady state levels 8 h after administration, and the tumor uptake was (almost by 6-times) faster for Trastuzumab-labeled liposomes against HER2/neu overexpressing SKOV3 tumors compared to liposomes without conjugated antibodies.

The biodistribution of ^{225}Ac delivered by immunolabeled MUVELs was compared to the following structures (constructs) containing ^{225}Ac: (a) immunolabeled large shell liposomes with encapsulated ^{225}Ac in their aqueous phase, (b) small vesicles with encapsulated ^{225}Ac in their aqueous phase and without conjugated antibodies on their surface, and (c) Trastuzumab-antibody conjugated to ^{225}Ac. The radioactivity distribution is represented as the tissue-to-kidney activity concentration ratio, since kidneys are the dose-limiting organ for ^{225}Ac due to ^{213}Bi selective accumulation. Among the different liposomal structures that were used to specifically deliver ^{225}Ac to cancer cells *in vivo*, multivesicular immunoliposomes showed the highest tumor-to-kidney uptake at both time points studied (Figure 6A). Four hours after administration the tumor-to-kidney ratio for multivesicular immunoliposomes was 6.9 ± 2.1 (black bars) and twenty-four hours later it further increased to 9.8 ± 4.4 (white bars). MUVELs exhibited significantly slower kinetics of tumor uptake compared to radiolabeled trastuzumab. The antibody demonstrated high initial tumor ratio of 15.5 ± 3.3 at 4 h, which decreased to 11.7 ± 0.6 24 h later. At that time point, the measured ^{225}Ac ratios at the tumor delivered by MUVELs and the radiolabeled antibody were not significantly different. Kidney and blood uptake of ^{225}Ac was low for all structures at the time intervals tested. The accumulation of radioactivity to the spleen at a significant extent, and to the liver, at a lesser degree, is consistent with reported values of liposome localization and probably does not reflect antibody targeting.

The biodistributions of ^{213}Bi, the last α-emitting daughter, was also evaluated for all constructs. Figure 6B shows the radioactivity distribution of ^{213}Bi as the tissue-to-kidney activity concentration ratio. At both time points (4 and 24 hours after administration), multivesicular immunoliposomes exhibited the highest tumor-to-kidney ratios among all other liposomal structures and the radiolabeled antibody.

FIGURE 6A

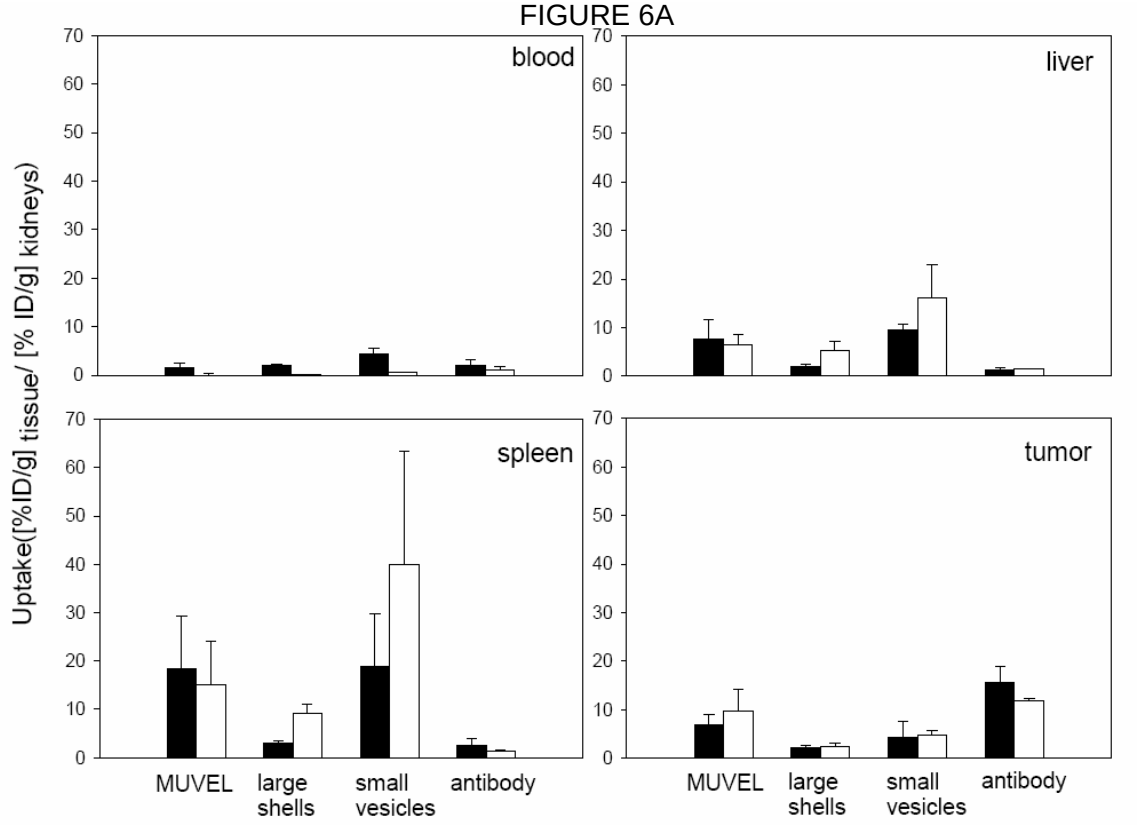

FIGURE 6B

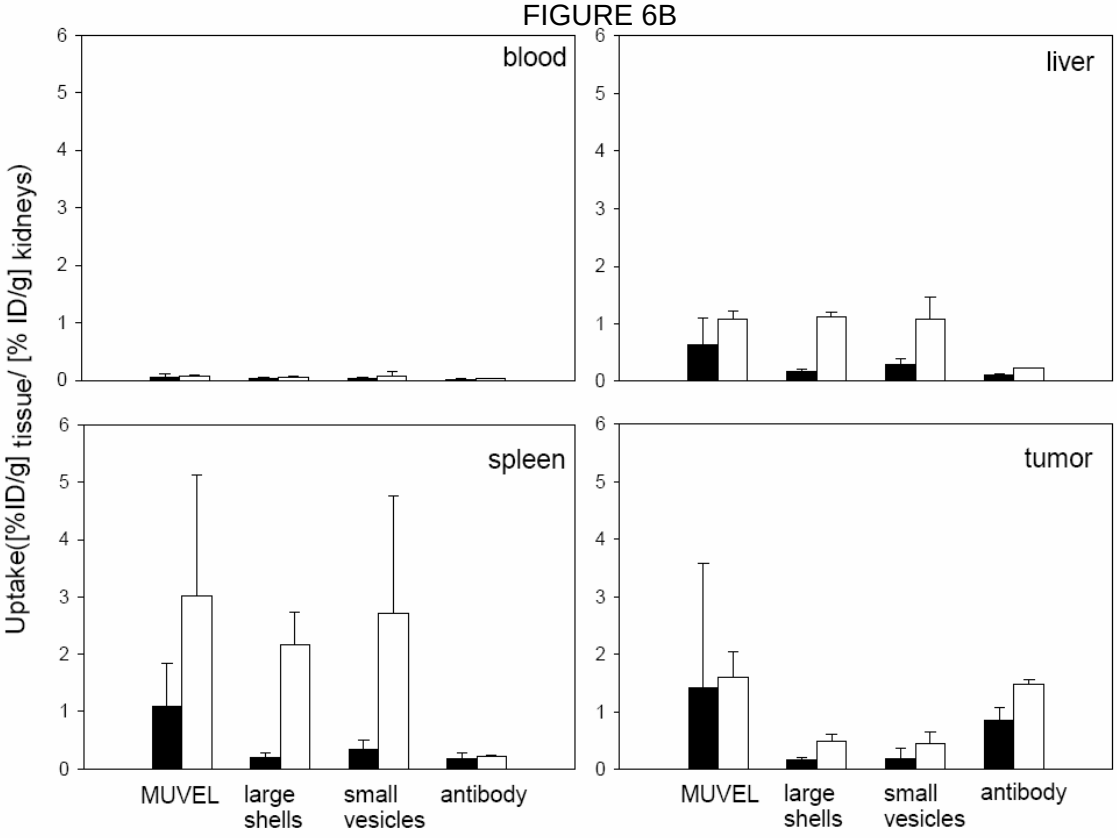

In vivo, the tumor uptake kinetics of ^{225}Ac mediated by MUVELs were significanlty slower than the accumulation observed for the radiolabeled antibody. Tumor uptake was comparable for the two constructs only 24 hours after administration. Due to the increased residence time of MUVELs in the IP cavity, a further increase with time of ^{225}Ac tumor accumulation mediated by MUVELs should be expected. In liposome administered animals, the measured whole body activities are greater than the sum of activities from the excised organs, suggesting prolonged retention (of ≈ 50%) of the injected liposome-associated activity in the peritoneal cavity (free ^{225}Ac-DOTA is rapidly cleared from the body). Direct sampling and characterization of peritoneal fluid was not performed. The slower peritoneal clearance of liposomes compared to the fast clearance of radiolabeled antibodies (33) could be a potential advantage for immunolabeled MUVELs with entrapped long-lived -particle emitters decaying to multiple -particle emitting daughters in localized treatments. Liposomes would, therefore, provide a longer available time to diffuse within the peritoneal cavity, allowing for greater tumor uptake over a prolonged time-peroid.

Comparison between the ratios of ^{213}Bi- to ^{225}Ac- activities at the tumor site for immunolabeled MUVELs and radiolabeled antibodies have been obtained (Figure 6C). Although MUVELs retained 18% of the ^{213}Bi daughter, this did not translate to a significant improvement in the tumor to kidney ^{213}Bi activity concentration ratio at 4 and 24 h after injection. This can be explained by the higher localization of MUVELs to liver and spleen relative to the radiolabeled antibody. Tumor localization of MUVELs will lead to MUVEL internalization by targeted tumor cells and therefore enhanced retention of Bi-213 at the tumor site. Localization to spleen and liver, on the other hand is likely to lead to MUVEL catabolism and release of free ^{225}Ac and, therefore, free ^{213}Bi. A reduction in spleen and liver MUVEL localization, by pre-injection of non-specific, non-radioactive liposomes would shift the biodistribution towards the tumor leading to enhanced retention of ^{213}Bi at the tumor site relative to ^{225}Ac-labeled antibody. Furthermore, since the relevant quantity regarding tumor control is the time-integrated delivery of alpha-particles over the effective lifetime of ^{225}Ac, the ratios at 4 and 24 hrs are not necessarily indicative of therapeutic effect relative to renal toxicity.

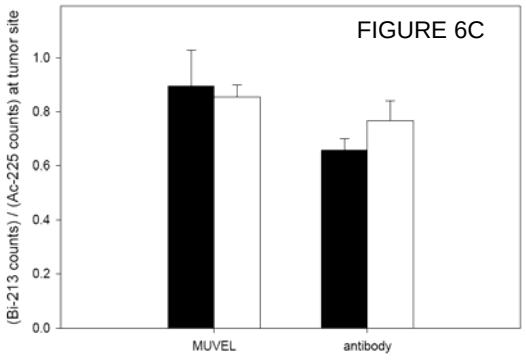

In figure 6c, values closer to unity, signify that less ^{213}Bi has escaped from the tumor or the delivery/targeting construct bound to the tumor. Enhanced retention of -particle emitting daughters by the targeted cancer cells will increase the killing efficacy of ^{225}Ac. For MUVELs the ratio does not significantly change over time and is closer to 0.89 for both time points. This value agrees with the *in vitro* cell-binding studies that showed high internalization fraction (83%) for cell-bound MUVELs and the significant retention of ^{213}Bi by MUVELs. For the radiolabeled antibody, the ^{213}Bi activity relative to the ^{225}Ac activity delivered at the tumor increases with time from 0.66 at four hours to 0.76 at

twenty-four hours post-administration. This result agrees with the fast binding kinetics of the radiolabeled antibody combined with fast clearance of the antibody from the peritoneal cavity (33). Since -particles originating on the cell surface have only an estimated 30% probability of traversing the cell nucleus (34), the high internalization extent of cell-bound MUVELs is a positive characteristic of this approach.

Finally, the radiation dose that can actually be delivered at the tumor sites would be substantially increased by MUVELs, especially for cancer cells that express relatively low levels of the targeted surface antigens (35). Radiolabeled antibodies with ^{225}Ac have generally low specific activity (0.038 mCi/mg in this study) that corresponds to one conjugated ^{225}Ac atom per 2,300 antibodies. With the current entrapment strategy, for MUVELs, two passive entrapment steps are required (each with a maximum of 10% encapsulation efficiency). Thus, for 1mCi ^{225}Ac initial activity, and 1% actinium overall entrapment efficacy, we can achieve one encapsulated ^{225}Ac nuclide per 8.7 MUVELs (assuming $4x10^{12}$ liposomes with a mean diameter of 750nm). Increase of the initial activity to 10 mCi ^{225}Ac should result in one actinium nuclide per MUVEL and two actinium nuclides in every 8 MUVELs. Thus, higher effective delivered dose at the tumor can, in principle, be reached using MUVELs. Current work is focused on increasing the encapsulated ^{225}Ac activity within small vesicles using active (ionophore-driven) loading. Further structural optimization of MUVELs is also required, to further increase the retention of radioactive daughters at the liposome sites and to minimize renal accumulation of free radioactive daughters.

The *in vivo* studies showed significant spleen uptake of MUVELs that may potentially affect the dosimetry and therapeutic potential of this approach. The impact of such localization on toxicity will require MTD studies. It is important to note that the relatively short range of -particles (80-100 m, or approximately 5 cell diameters), and their microscopic distribution in the spleen may mitigate potential toxicity. There is evidence that liposomes are taken up by splenic macrophages rather than parenchymal splenic cells (36). Similarly, regarding the liver uptake, liposome accumulation may be attributed to opsonin-mediated uptake by Kupffer cells at the endothelial hepatic sites, without reported penetration into the parenchymal region. Also, as noted above, the administration of non-specific, non-radioactive liposomes prior to the MUVELs could reduce uptake by the reticuloendothelial system (RES) and increase MUVEL localization to the target site. Such an approach to reduce RES uptake has been previously demonstrated ().

Intraperitoneal micrometastatic disease constitutes a treatment challenge. In this work, the ovarian carcinoma model was selected as a proof of principle for delivery of the -particle nanogenerator ^{225}Ac to disseminated intraperitoneal micrometastases using MUVELs and locoregional administration. Our findings suggest that radioimmunolabeled MUVELs could potentially reduce the toxicity associated with the untargeted radioactive daughter emissions of ^{225}Ac while increasing delivery of -particle emissions per targeted cells, providing a promising therapeutic modality for disseminated micrometastatic disease. Additional optimization of these structures is necessary.

KEY RESEARCH ACCOMPLISHMENTS

- Sterically stabilized, PEGylated and immunolabeled (with Herceptin antibody) multivesicular liposomes (MUVELs) have been generated to increase retention of ^{213}Bi.
- Their size distribution has been evaluated by dynamic light scattering and electron microscopy.
- Specific targeting and endocytosis of MUVELs has been demonstrated, *in vitro*.
- Biodistribution following intraperitoneal injection in tumor-free and tumor-bearing mice using gamma counting, with ^{111}In-labeled liposomes has been evaluated.
- Liposomal loading with ^{225}Ac has been achieved.
- The retention of ^{225}Ac and ^{213}Bi (the last alpha-emitting daughter in the decay chain) have been evaluated and shown to be substantially greater than the previously reported constructs (98% vs 88% for ^{225}Ac at 30 days and 18% vs 5% for ^{213}Bi at 30 days.
- The biodistribution of ^{225}Ac-loaded MUVELs was compared to ^{225}Ac-labeled antibody in tumor-bearing mice

REPORTABLE OUTCOMES

Sofou S, Enmon RM, Palm S, Kappel B, Zanzonico P, McDevitt MR, Scheinberg DA, Sgouros G. Large radioimmunoliposomes for targeted intraperitoneal therapy of metastatic cancer: binding, internalization and biodistribution studies. Manuscript to be submitted to JNM (this manuscript was rejected by JNM and will be resubmitted once the reviewer criticisims are addressed)

Sofou S, Kappel B, Jaggi JS, McDevitt MR, Scheinberg DA, Sgouros G. Enhanced Retention of the α-particle Emitting Daughters of Actinium-225 by Engineered Liposomal Carriers for Targeted Therapy of Micrometastatic Cancer. Manuscript to be submitted to Cancer Research.

CONCLUSIONS

Because of the low ^{213}Bi retention obtained with simple large antiHER2/neu radioimmunoliposomes, we have engineered previously unreported structures, MUVELs designed to address the known reasons for the low ^{213}Bi retention. Although not as large as expected theoretically, the MUVEL structures increased ^{213}Bi retention from 5% to 18%. MUVELs were shown to rapidly and effectively target intraperitoneal tumors in an ovarian carcinoma animal model. The advantage in ^{213}Bi retention in the tumor relative to the kidneys (the site of free ^{213}Bi localization) was not as high as expected and this is believed to be due to the high accumulation of MUVELs in the spleen, and to a lesser extent, the liver. Pre-injection of unlabeled MUVELs will be considered to saturate these sites and increase MUVEL localization to tumor.

In the next year we will focus on increasing the efficiency of ^{225}Ac encapsulation into MUVELs using an ionophore loading methodology. The loaded liposomes will then be used to in toxicity and tumor kill studies, *in vivo*. Despite the lower than expected retention of ^{213}Bi at the tumor site, we believe that pre-injection with unlabeled liposomes will resolve this by shifting localization away from the spleen and to the tumor where a greater fraction of the administered MUVELs will be internalized and the Bi-213 entrapped intracellularly. It is also important to note that MUVELs can deliver a greater number of alpha-particles to the tumor cell per vehicle than can antibodies.

"So What?"

The work performed in the second year of this grant has improved upon the results previously obtained and allowed us to move a step closer to delivery of actinium-225 and its daughters to ovarian carcinoma metastases in the peritoneal cavity. Since liposomes clear from the peritoneal cavity much more slowly than antibodies, targeting to cancer cells is improved and the ratio of absorbed dose to tumor cells versus normal organs is likewise improved. This makes it possible to administer greater levels of radioactivity for cancer therapy. In the next year the efficacy and toxicity of alpha-particle emitter containing radioimmunoliposomes will be evaluated in an ovarian carcinoma model system.

REFERENCES

1. Sofou S, Thomas JL, Lin H, McDevitt MR, Scheinberg DA, Sgouros G. Engineered liposomes for potential α-particle therapy of metastatic cancer. J Nucl Med 2004; 45:253-260.

2. Sofou S, Enmon RM, Palm S, Kappel B, Zanzonico P, McDevitt MR, Scheinberg DA, Sgouros G. Large radioimmunoliposomes for targeted intraperitoneal therapy of metastatic cancer: binding, internalization and biodistribution studies. Manuscript to be submitted to JNM. (included in Appendix)

3. Sofou S, Kappel B, Jaggi JS, McDevitt MR, Scheinberg DA, Sgouros G. Enhanced Retention of the α-particle Emitting Daughters of Actinium-225 by Engineered Liposomal Carriers for Targeted Therapy of Micrometastatic Cancer. Manuscript to be submitted to Cancer Research. (included in Appendix)

Appendix

1. Sofou S, Enmon RM, Palm S, Kappel B, Zanzonico P, McDevitt MR, Scheinberg DA, Sgouros G. Large radioimmunoliposomes for targeted intraperitoneal therapy of metastatic cancer: binding, internalization and biodistribution studies. Manuscript to be submitted to JNM.

2. Sofou S, Kappel B, Jaggi JS, McDevitt MR, Scheinberg DA, Sgouros G. Enhanced Retention of the α-particle Emitting Daughters of Actinium-225 by Engineered Liposomal Carriers for Targeted Therapy of Micrometastatic Cancer. Manuscript to be submitted to Cancer Research.

Large Radioimmunoliposomes for Targeted Intraperitoneal Therapy of Metastatic Cancer: Binding, Internalization and Biodistribution Studies

Stavroula Sofou, PhD[1]; Richard Enmon, PhD[1]; Stig Palm, PhD[*]; Barry Kappel, B.A.[1]; Pat Zanzonico, Ph.D.[2]; Michael R. McDevitt, PhD[1]; David A. Scheinberg, MD, PhD[1]; and George Sgouros, PhD[3].

Program in Molecular Pharmacology and Chemistry (1), Department of Radiology, Nuclear Medicine Service (2), Memorial Sloan-Kettering Cancer Center, 1275 York Ave, New York, NY 10021,
Department of Radiology (3), Division of Nuclear Medicine, Johns Hopkins Medicine, 220 Ross Research Building, 720 Rutland Ave, Baltimore, MD 21205

*Present address: Department of Radiation Physics, Göteborg University, Sweden

Key words: large immunoliposomes, trastuzumab, intraperitoneal radiotherapy, ovarian cancer

Work supported by the USAMRMC Concept and IDEA Awards DAMD170010657, and DAMD170310755, respectively. Also supported by NIH R01 CA55349, the Experimental Therapeutics Center, and the Goodwin Commonwealth Foundation for Cancer Research. D.A.S. is a Doris Duke Distinguished Science Professor. S.S. is the recipient of Dr. Frederick E.G. Valergakis Graduate Research Grant of the Hellenic University Club of New York

Running title: “Large immunoliposomes for radiation therapy”

ABSTRACT

Effective targeting and sterilization of intraperitoneally (IP) disseminated micrometastases remains a challenge. In this work we examine the potential of large immunoliposomes as vehicles for IP-delivery of radiation. Such radioimmunoliposomes combine the targeting efficacy of the surface-conjugated tumor-specific antibodies, with the long retention time of large liposomes in the peritoneal cavity. This could result in enhanced tumor targeting, increased tumor irradiation and minimal toxicity to normal organs.

Methods: 500 to 800 nm-diameter, zwitterionic and cationic liposomes were conjugated to trastuzumab, an anti-HER2/neu antibody. Retention of liposome content was evaluated, *in vitro*. ^{111}In-DTPA was entrapped into liposomes and the binding and internalization of radioimmunoliposomes to SKOV3, a HER2/neu-positive ovarian carcinoma cell line, was tested. The biodistribution and pharmacokinetics of ^{111}In-DTPA-containing liposomes were determined by imaging and tissue counting of radioactivity in tumor-free and SKOV3-tumor-bearing mice after IP administration of the radiolabeled liposomes.

Results: Large, stable, PEGylated radioimmunoliposomes of different charge were prepared. ^{111}In-DTPA was successfully and stably entrapped in liposomes. Content retention by liposomes in media and ascites fluid was high (> 53% after 20 days). *In vitro* binding of radioimmunoliposomes, after 4 hours of incubation, increased 16-fold for the zwitterionic and 53-fold for the cationic immunoliposomes compared to non-targeted liposomes.

Internalized radioactivity was greater than 56% of the cell-associated radioimmunoliposomes, and depended on the type of liposomes used and the incubation time. Studies, performed *in vivo*, demonstrated the following: At four hours post-injection, tumor uptake was 17.6±3.7%ID/g and 21.3±19.5%ID/g for zwitterionic and cationic radioimmunoliposomes, respectively. Fluorescent liposomes were detected in intact form in the peritoneal cavity 6 hours after administration. Significant liver (3.9–24.9%ID/g) and spleen (130.6–296.3%ID/g) accumulation was observed at eight hours after administration.

Conclusions: This work demonstrates *in vitro* binding and internalization of large liposomes with prolonged intracellular retention of encapsulated radioactivity. Tumor targeting and prolonged retention following IP administration was seen, as well as significant liver and spleen accumulation. Because large radioimmunoliposomes are cleared from the peritoneal cavity relatively slowly, encapsulation of radionuclides with short half-lives would preferentially irradiate tumor cells with minimal normal organ irradiation. In addition, the high tumor targeting within the peritoneal cavity suggests that encapsulation of radionuclides with short-range emissions (e.g. alpha-particles) would spare surrounding normal tissue while delivering a sterilizing absorbed dose to disseminated peritoneal micrometastases.

Keywords: large immunoliposomes, trastuzumab, intraperitoneal radiotherapy, ovarian cancer

INTRODUCTION

Micrometastatic dissemination in the peritoneal cavity remains a treatment challenge for patients with gastrointestinal and gynecological cancers. A promising approach for the therapy of peritoneally disseminated cancer is intraperitoneal (IP) administration of therapeutic agents. The rationale for intraperitoneal administration is twofold. First, it is a direct way to access peritoneally disseminated disease. High concentrations of the therapeutic moiety can be achieved in the peritoneal cavity, before its concentration reaches toxic levels in the dose-limiting organs *(1,2)*. Second, micrometastatic tumors in the peritoneal cavity may have not developed vasculature *(3)*. For these particular cases, intravenous administration of therapeutics will not be the optimal route to target intraperitoneal micrometastases. An effective therapy for micrometastatic tumors is of great importance because disseminated micrometastatic disease is rarely cured by current treatment options.

We studied the potential of IP administered radioimmunoliposomes for targeting and irradiation of micrometastatic cancer in the peritoneal cavity. Liposomes are closed shell structures defined by a phospholipid bilayer membrane that encloses an aqueous compartment *(4)*. We use the term ‘radioimmunoliposomes’ to describe those liposomes in which the internal compartment encloses radioactive elements and, the surface is conjugated with tumor-specific antibodies. Clinical trials have demonstrated that IP-administered radioimmunotherapy could be advantageous in cases of small

volume disease *(5-7)*. Also, clinical trials on liposomally entrapped chemotherapeutic agents for IP therapy show encouraging results due to prolonged retention of liposomes in the peritoneal cavity *(8,9)*.

Conjugation of multiple numbers of targeting antibodies per liposome should enhance binding of liposomes to the targeted tumor sites *(10,11)*. Because of their large size, liposomes would be expected to have extended retention in the peritoneal cavity and, consequently, to have more time to interact with tumor targets. The retention half-life in the peritoneal cavity of humans for IP administered antibodies is 30 to 67 hours *(12)*. In contrast, the peritoneal concentration of chemotherapeutics after IP administration of their liposome based formulations, has been shown to decrease by less than 10% during the first 48 hours *(9)*. Lastly, because the enclosed aqueous compartment of liposomes can be used to entrap up to 10^3-10^6 water soluble molecules, radiolabeling efficiency of liposomes does not present a constraint, compared to radiolabelled antibodies where high radioconjugation levels may interfere with the antibody immunoreactivity *(13)*.

In this study, large radioimmunoliposomes were evaluated for targeting peritoneally disseminated tumors in an animal model of ovarian carcinoma. Ovarian cancer has the highest mortality among gynecological malignancies. Epithelial ovarian cancer, in the majority (70%) of patients, is first detected as a result of symptoms arising after the disease has spread outside of the pelvis and into the peritoneal cavity. In such cases of advanced disease (FIGO-Stage III), the 5-year survival rate employing current treatment approaches is

approximately 15 to 20%. These data suggest that a new treatment modality is needed for disseminated epithelial ovarian carcinoma.

Large, PEGylated liposomes of different surface charge (zwitterionic and cationic) were engineered and indium-111, a gamma-emitting radionuclide with a 67-h half-life, was entrapped within liposomes. Liposomes were then labeled with the monoclonal antibody Trastuzumab, which specifically targets the HER2/neu epidermal growth factor receptor that is overexpressed in the SKOV3 ovarian carcinoma cell line. After characterizing the biodistribution and pharmacokinetic profile of IP administered large liposomes in tumor-free mice, the tumor uptake of radioimmunoliposomes was determined in tumor bearing mice.

Large zwitterionic and cationic anti-HER2/neu radioimmunoliposomes demonstrated rapid localization in the peritoneal tumors with higher tumor uptake than corresponding liposomes not labeled with antibodies. Also, at least 6 hours after administration, intact liposomes are still present in the peritoneal cavity. The findings of this study suggest that intraperitoneally administered large radioimmunoliposomes warrant further investigation as a potential strategy for therapy of intraperitoneal metastatic cancer.

MATERIALS AND METHODS

Reagents

The lipids L-α-phosphatidylcholine (egg) (EPC), 1,2-dipalmitoyl-sn-glycero-3-phosphoethanolamine-N-[methoxy(polyethyleneglycol)-2000] (ammonium salt) (PEG-labeled lipid), 1,2-dipalmitoyl-sn-glycero-3-ethylphosphocholine (chloride salt) (cationic lipid), L-α-phosphatidylethanolamine-N-(4-nitrobenzo-2-oxa-1,3-diazole) (egg) (NBD-PE), L-α-phosphatidylethanolamine-N-(lissamine rhodamine B sulfonyl) (egg) (rhodamine-PE), 1,2-distearoyl-*sn*-glycero-3-phosphoethanolamine-N-[maleimide (polyethylene glycol) 2000] (ammonium salt) (maleimide-PE) (purity >99%) were purchased from Avanti Polar Lipids (Alabaster, Al). Cholesterol, phosphate buffered saline (PBS), fluorexon (calcein), Sephadex G-50, diethylenetriaminepentaacetic acid (DTPA), 8-hydroxyquinoline (oxine), ascorbic acid, Triton X-100, and the control ascites fluid from murine myeloma were purchased from Sigma-Aldrich (St. Louis, MO). Dithionite (sodium hydrosulfite, tech. ca. 85%) was obtained from Acros Organics (NJ). Traut's reagent (2-Iminothiolane-HCl) was purchased from Pierce (Rockford, IL). Indium-111 was obtained from PerkinElmer Life Sciences Inc. (Boston, MA).

Liposome preparation

Mixtures of phosphatidyl choline (EPC), cholesterol (1:1 molar ratio), and PEG-labeled lipids (5.3 mole % of total lipid) in $CHCl_3$ were dried in a rotary

evaporator (for cationic liposomes, cationic lipid was included in 10 mole % of total lipid). For stability measurements, the lipids were resuspended in calcein solution (55 mM calcein in phosphate buffer, isosmolar to PBS, pH=7.4). For ^{111}In passive entrapment, the lipids were resuspended in PBS containing chelated indium complexes (^{111}In-DTPA, 3.7-37 MBq per ml). The lipid suspension was then annealed to 55^{o}C for 2 hours *(14)*. To make liposomes, the lipid suspension was then taken through twenty-one cycles of extrusion (LiposoFast, Avestin, Ontario, Canada) through two stacked polycarbonate filters (800 nm filter pore diameter), and unentrapped contents were removed by size exclusion chromatography (SEC) in a Sephadex G-50 (Aldrich, St. Louis, MO) packed 1x10 cm column, eluted with a PBS isotonic buffer. For ^{111}In encapsulating liposomes, 1mM DTPA was added to the liposome suspension 30 minutes prior to SEC. Also, a chemical method was followed to load ^{111}In into preformed liposomes. The loading protocol for indium is published elsewhere *(15)*. Briefly, to 1 ml of preformed liposomes, with entrapped 2mM DTPA, we added drop-wise 100 µl of $InCl_3$ in 3 mM HCl and 100 µl of oxine in 1.8 wt % NaCl / 20mM sodium acetate (3 µl of 11 mM oxine in EtOH added to the acetate buffer, pH=5.5). After loading, unentrapped ^{111}In was complexed with externally added 2mM EDTA and was separated from the liposomal suspension by SEC in a Sephadex G-50 packed 1x10 cm column, eluted with phosphate buffer (PBS, pH=7.4). Ascorbic acid (8 mmol/l) was coentrapped to minimize lipid oxidation due to radiation *(16)*.

Retention of entrapped contents by liposomes

To study the retention of entrapped contents by liposomes, a fluorescent dye (calcein) was encapsulated at self-quenching concentrations. Liposome stability was determined in PBS, in RPMI 1640 medium supplemented with 1-10% fetal calf serum (Sigma-Aldrich), and in murine ascites fluid (Sigma-Aldrich) at 37^{o}C over time. The fluorescence intensity of liposome suspensions was measured by a fluorescence microplate reader (ex: 485 nm; em: 538 nm). Destabilization of the liposomal membrane causes calcein leakage from the liposomes. Calcein leakage is followed by dilution of calcein into the surrounding solution and relief of the fluorescence self-quenching effect, which results in increase of fluorescence intensity. To normalize and properly compare different samples, Triton X-100 (4.5% wt /wt) was added into the suspension to achieve complete calcein release. To quantitate liposome stability, the fluorescence self-quenching efficiency q of liposome suspensions was compared over the period of 30 days ($q=I_{max}/I$, where I is the measured fluorescence intensity before Triton X-100 addition, and I_{max} the maximum fluorescence intensity after Triton X-100 addition).

To determine the retention of ^{111}In by liposomes, DTPA was added for 30 minutes into a fraction of the liposome suspension, and after SEC, the γ-emissions of ^{111}In retained by liposomes were measured using a Cobra γ-counter (Packard Cobra Gamma Counter, Packard Instrument Co., Inc., Meriden, CT). The energy window used for ^{111}In was 15-550 keV.

Liposome lamellarity

A dithionite assay was used to determine the lamellarity of the zwitterionic and cationic liposomes. Dithionite ion $S_2O_4^-$ and the spontaneously produced $^{\cdot}SO_2^-$ radical react with the NBD-PE labeled lipids of the outer membrane layer and produce non-fluorescent derivatives *(17)*. They diffuse very slowly through the bilayer and thus allow the quantitative distinction of the inner and outer layer lipids. In our NBD-PE labeled vesicle preparations unilamellarity was verified by a 53 ± 0.1 % (zwitterionic liposomes) and 52 ± 0.2 % (cationic liposomes) decrease of the initial fluorescence upon dithionite addition.

Liposome size distribution determination

Dynamic light scattering (DLS) of liposome suspensions was studied with an N4 Plus autocorrelator (Beckman-Coulter), equipped with a 632.8 nm He-Ne laser light source. Scattering was detected at 15.7^o, 23.0^o, 30.2^o, and 62.6^o. Particle size distributions at each angle were calculated from autocorrelation data analysis by CONTIN *(18)*. The average liposome size was calculated to be the y-intercept at zero angle of the measured average particle size values vs $\sin^2(\theta)$ *(19)*. All buffer solutions used were filtered with 0.22 μm filters just prior to liposome preparation. The collection times for the autocorrelation data were 1-4 minutes.

Liposome immunolabeling

Trastuzumab (5-10 mg/ml, in PBS, pH=8) was purified from Herceptin® (Genentech, South San Francisco, CA) and was reacted with Traut's reagent for 1 hr at room temperature under a nitrogen atmosphere. Then the antibody was purified by size exclusion chromatography in a 10DG column (Biorad, Hercules, CA) eluted with PBS (with 1mM EDTA, pH=7.4). An average of 5-7 sulfhydryl groups per antibody were determined using the Ellman's assay and a protein assay (DC protein assay, Biorad). Liposomes (7-15 mM lipid) containing maleimide-PE (1 mole% of total lipid) were then incubated with antibody solution (0.5-5 mg/ml) overnight at room temperature under N_2. After completion of conjugation, excess maleimide groups were quenched with β-mercaptoethanol (3:1 molar ratio) for 30 minutes. Immunoliposomes were purified from unreacted antibody and β-mercaptoethanol by size exclusion chromatography in a 4B stationary phase (Sigma-Aldrich) packed 1x10 cm column, eluted with PBS. A protein assay was used to quantify the concentration of antibodies in the liposome suspension. Lipid concentration was determined by the fluorescence intensity of rhodamine-PE containing liposomes (0.5-1 mole% of total lipid). The average number of antibodies per liposome was estimated using the assumption that for 650 nm diameter liposomes, and 70$Å^2$ head group surface area per lipid *(20)*, a liposome would consist of an average of 3.7 million lipid molecules.

Cell culture and Tumor inoculation

Stock T-flask cultures of the human ovarian carcinoma cell line SKOV3-NMP2 *(2)* were propagated at 37^{o}C, in 5% CO2 in RPMI 1640 media supplemented with 10% fetal calf serum (Sigma-Aldrich), 100 units/ml penicillin, and 100mg/ml streptomycin. Cell concentration was determined by counting trypsinized cells with a hemocytometer. Tumor inoculation was prepared from a single cell suspension in DME medium (Dulbecco's Modified Eagle's Medium). Each 4-6 week old female Balb/c nude mouse (Taconic, Germantown, NY) received 0.15-0.20 ml inoculum of $5x10^6$ cells administered by intraperitoneal injection.

Mice were housed in filter top cages and provided with sterile food and water. Animals were maintained according to the regulations of the Research Animal Resource Center (RARC) at Memorial Sloan-Kettering Cancer Center (MSKCC), and animal protocols were approved by the Institutional Animal Care and Use Committee (IACUC).

Cell Binding and internalization of liposomes

Flow cytometry was used to determine the specific binding of liposomes to SKOV3 cells. The liposomal membrane was labeled with the fluorescent lipid rhodamine-PE (excitation: 550 nm; emission: 590 nm). Harvested SKOV3 cells were washed three times with ice-cold buffer (PBS/ 0.5% BSA/ 0.02% NaN_3) and then resuspended at a density of $5.6x10^6$ cells/ml. 10^6 cells were incubated on ice with liposomes for 25 minutes (3.3 mM final lipid

concentration), then washed three times and finally resuspended at a density of $2.5x10^6$ cells/ml. To determine the extend of specific binding of immunoliposomes to the HER2/neu antigen receptor, cells were also preincubated with Trastuzumab at 5μg of antibody per one million cells for 25 minutes on ice. Cells were then washed twice with ice-cold buffer and incubated with liposomes as above. Fluorescence counting of cell suspensions was measured using a Beckman-Coulter Cytonics FC500 flow cytometer (Fullerton, CA), and analyzed with the software FlowJo (Tree Star, Inc., Ashland, OR).

To quantitate cell binding and internalization of liposomes, harvested SKOV3 cells were washed twice with ice-cold media (RPMI 1640/ 10% FBS/ 2% BSA) and then resuspended in cold media (as above) at a density of 10^6 cells/ml. Radiolabeled liposomes (250 μl of 1.8mM lipid) were added to 3.5 ml of cell suspension and two 200μl samples were immediately taken and processed as described below. The cells were then placed in a humidified, 37^oC incubator with 5% CO_2, where they were periodically swirled and sampled at 0.5, 1, 2, 4, and 24 hrs. The cells were washed three times with 2ml of ice-cold PBS, and then 1ml of an acidic striping buffer (50 mM glycine, 150 mM NaCl, pH=2.8) was added for 10 minutes at room temperature to eliminate the charge-specific binding of membrane bound conjugates and to remove the surface bound immunoliposomes. After centrifugation, the supernatant and pellet were counted, and the percentages of membrane-bound and internalized counts were determined.

Excised organ quantitation

Mice were injected IP with liposomes (0.1-0.2 ml suspension, 1.4 μmole total lipid) with entrapped ^{111}In, and were sacrificed at different time points post-injection by CO_2 intoxication for dissection. The average activity per inoculum was 37 kBq. The whole body clearance was measured with a dose calibrator (Model CRC-15R, Capintec, NJ). Blood was collected via cardiac puncture. Organ and muscle tissues were washed in PBS and weighed. The samples were then counted for photons in a gamma-counter. Results were expressed for each organ as percentage of total radioactivity injected, divided by the organ mass (%ID/g). A bi-exponential curve of the form $A_1*\exp(-t*\ln(2)/T_1))-A_2*\exp(-t*\ln(2)/T_2))$ was applied to fit the uptake and clearance phase of the blood kinetics, using a commercial software program (SigmaPlot,, SPSS Inc.).

Gamma camera imaging

Mice were injected intraperitoneally with 0.1-0.4 ml liposome suspensions with encapsulated ^{111}In and average activity per inoculum 0.74-1.48 MBq. Each mouse was imaged with a planar gamma camera using the small-animal X-SPECT Imaging system (Gamma Medica Inc., Northridge, CA). Time dependent distribution and localization of liposomes were determined by four imaging sessions over the course of 24 hours. During imaging, the mice were

kept anesthetized using an isoflurane (Forane) (Baxter, Deerfield, IL) loaded vaporizer.

Mice fluorescent imaging

To image intact liposomes in the peritoneal cavity, mice were injected with liposomes containing an encapsulated fluorophore (calcein) at self-quenching concentrations. Mice were anesthetized at 6 or 48 hours post-injection using 100 mg/kg ketamine, 10 mg/kg xylazine, and were then sacrificed by cervical dislocation. The peritoneal cavity was exposed after removal of the abdominal skin and the peritoneal membrane, and fluorescent images of the peritoneal cavity were acquired before and after addition of Triton X-100, which disrupts the liposomal membranes and causes relief of calcein self-quenching. Mice were digitally imaged using an ORCA CCD camera fitted with a macro-lens (Hamamatsu, Hamamatsu City, Japan) and MCID 5+ imaging software (Imaging Research, Ontario, Canada). Two mice were imaged per time point for each of the two liposome suspensions injected (zwitterionic, cationic). Fluorescent images were acquired using an Illunatool Tunable Lighting System, 470nm +/- 20nm exciter filter and 525nm +/- 20nm barrier filter (Lightools, Encinitas, CA).

RESULTS

Liposome characterization

The measured average liposome sizes for the zwitterionic composition was 646 ± 288 nm (diameter) on the day of preparation and 657 ± 365 nm after 30 days. For the cationic composition the corresponding values were 602 ± 385 nm and 678 ± 357 nm, respectively.

To evaluate the stability of liposomes over time, in terms of content retention, calcein (a self-quenching fluorophore) was entrapped into liposomes at high concentrations. Release of calcein, due to membrane instability, results in dilution of the fluorophore by the surrounding solvent, relief of self-quenching, and increase of the fluorescence intensity. The fractional fluorescence self-quenching decrease, $\Delta q \times 100$, is shown on tables 1 and 2 for zwitterionic and cationic liposomes over the period of 30 days at 37^{o}C in media (with 1-10% serum) and in ascites fluid, respectively. Incubation of liposomes in media resulted, after the first 24 hours, in a maximum of 17% decrease in self-quenching, which possibly could be attributed to differences in osmolarity between the encapsulated calcein solution and the liposome surrounding solvent. Beyond this point liposomes were generally stable for over 30 days (Table 1). In ascites fluid, after 15 days of incubation, a 21% decrease in self-quenching was measured for zwitterionic liposomes, and no decrease was observed for cationic liposomes. After incubation for 30 days in ascites fluid, more than 50% decrease in self-quenching was observed for both zwitterionic and cationic liposomes.

Retention of ^{111}In by liposomes

The efficiency of ^{111}In entrapment in liposomes was 5-10% and 73-81% with the passive and chemical loading method, respectively.

The decay-corrected ^{111}In activity that was retained in the zwitterionic and cationic liposomes three days after preparation was >88% and > 87% of the liposome initial activity (on the day of preparation) for the liposomes that were loaded with the passive and chemical method, respectively.

Liposome immunolabelling

The conjugation reaction resulted in 65-90 antibodies per zwitterionic liposome and 90-145 antibodies per cationic liposome. To determine the possible leakage of entrapped contents during conjugation, calcein was encapsulated into liposomes at self-quenching concentrations. No significant change in self-quenching efficiency was detected (data not shown).

Cell binding and internalization of liposomes

To determine binding of liposomes to SKOV3 cells, the liposomal membrane was labeled with a fluorescent phospholipid (rhodamine-PE, 1 mole % of total lipid), and cell suspensions were incubated with immunolabeled and plain liposomes. Also, in parallel measurements for the determination of the specific binding of immunoliposomes to the HER2/neu antigen receptor, SKOV3 cells were previously blocked with excess Trastuzumab, the antibody

that was also conjugated to immunoliposomes. Figure 1 shows the flow cytometry histograms for binding of zwitterionic immunoliposomes (Figure 1A) and plain liposomes (Figure 1B) to SKOV3 cells, respectively, with blocking (shaded gray) and without blocking (thick solid line) of the HER2/neu antigen receptor on the cell surface. A significant shift in fluorescence counts of SKOV3 cells was detected only in the case of immunoliposomes, and only when the HER2/neu receptors on the cell surface were not blocked (Figure 1A, thick solid line). Non-specific binding of plain zwitterionic liposomes to SKOV3 cells was not detected as is depicted by the unchanged fluorescence of cells in Figure 1B. Contrary to zwitterionic liposomes, cationic liposomes exhibit non-specific binding (Figure 1C for cationic immunoliposomes with blocked receptors: shaded gray, and Figure 1D for cationic plain liposomes with and without blocking: shaded gray and thick solid line). Binding of cationic immunoliposomes to unblocked SKOV3 cells showed the largest shift in cell fluorescence counts (Figure 1C: thick solid line).

SKOV3 cells were also incubated with TRIC-labeled antibodies. Trastuzumab (shaded black) but not Rituximab® (an irrelevant antiCD20 antibody, shaded gray) binds specifically to SKOV3 cells, as is shown in Figure 1E.

To quantitatively determine liposomal binding and internalization, liposomes with entrapped ^{111}In were incubated at 37^{o}C with SKOV3 cell suspensions for 0, 0.5, 1, 2, 4 and 24 hours. The total cell-associated radioactivity increased over time of incubation reaching at 4 hours a 4-fold increase for zwitterionic

immunoliposomes (Figure 2A) and a 29-fold increase for cationic immunoliposomes (Figure 2B) compared to the values for total cell-associated radioactivity of immunoliposomes at t=0. For zwitterionic immunoliposomes, internalized radioactivity increased 13-fold within the first 4 hours and then remained constant for up to 24 hours (24 hr. time-point not shown on plot). However, the total cell associated intensity continued to rise reaching a 6-fold increase after 24 hours. In other words, internalization and replacement on the cell membrane of the HER2/neu target receptor occurred only the first few hours of incubation. At later times, internalization of the receptor was diminished.

For cationic immunoliposomes, both the total cell-associated radioactivity and the internalized radioactivity increased over 24 hours of incubation (24 hour time point not shown on the plot). No saturation of receptor internalization was observed. At 24 hours, a 189-fold increase in cell-associated radioactivity was observed with a 111-fold increase in internalized counts. The increase in membrane bound activity implies that the HER2/neu target receptor was being replaced on the cell membrane after receptor internalization.

At 24 hours, 1.2% of the total zwitterionic and 13.3% of the total cationic immunoliposome activity was cell-associated. Non-targeted plain liposomes showed low, non-specific, cell-binding (Figures 2A and 2B). Only 0.3% of total zwitterionic and 0.9% of total cationic non-targeted liposome activity was cell-associated.

Biodistributions of large liposomes in tumor free mice

The biodistributions and pharmacokinetics of large zwitterionic and cationic plain liposomes, with entrapped ^{111}In-DTPA, were determined, initially, in Balb/c mice without tumor. At 1, 4, 8, and 24 hours post IP administration of liposomal suspensions, animals were killed and the radioactivity distribution of excised tissues was obtained by γ counting. The biodistributions of large zwitterionic and cationic plain liposomes in mice without tumor are shown in Figures 3A and 3B respectively. The most significant normal organ accumulation was in the liver and spleen. 4 hours post-injection of zwitterionic liposomes (Figure 3A) , 3.2 ± 1.3% ID/g and 68.8 ± 40.1% ID/g was accumulated in the liver and spleen, respectively, and at 8 hours the corresponding values were 3.9 ± 3.5% ID/g and 130.6 ± 197.9% ID/g. Cationic liposomes had higher uptake by the liver (Figure 3B). At 4 and 8 hours post-injection 11.2 ± 7.7% ID/g and 24.9 ± 4.5% ID/g of cationic liposomes was accumulated in the liver. The maximum uptake in the liver and spleen was observed 8 hours post-injection for both liposomal compositions.

The whole body clearance was low when liposomes were administered. Twenty-four hours post-administration, at least 73% of the initial whole body activity was retained. On the contrary, rapid whole body clearance was observed after administration of ^{111}In-DTPA (Figure 3C). Blood uptake and elimination kinetics of zwitterionic liposomes was described by a bi-exponential curve with mean half-lives of 0.51 ± 0.29 hours and 5.79 ± 0.24

hours, respectively. The corresponding values for cationic liposomes were 0.68 ± 0.84 hours and 2.74 ± 0.71 hours. At early time (1-4 hours), blood showed a significant uptake of 6-8% ID/g that may reflect a fraction of rapidly disrupted liposomes after intraperitoneal injection, or smaller size liposomes that escape the peritoneal cavity through lymphatic drainage.

Biodistributions of large zwitterionic liposomes in tumor bearing mice

Biodistributions of plain- and immuno- liposomes were determined in tumor bearing mice. Fourteen days after inoculation, a tumor pattern was formed, that consisted of nodules on the ventral side of the spleen. Smaller nodules (~ 1mm in diameter) were frequently observed within the mesentery. At 14 days post-innoculation, the mean weight of observed tumor nodules was 0.269 ± 0.242 g (n=30, total number of animals).

4 hours after IP administration of large zwitterionic liposomes the tumor uptake of immunoliposomes was 17.6 ± 3.7% ID/g, and only 2.7 ± 0.7% ID/g for plain non-targeted liposomes (Figures 4A and 4B). Twenty-four hours after administration, the difference in tumor uptake between the two liposomal groups was smaller: 12.0 ± 4.0% ID/g for immunoliposomes and 8.7 ± 6.1% ID/g for plain zwitterionic liposomes. The normal organ with the highest uptake was the spleen with 83.3 ± 19.7% ID/g for zwitterionic immunoliposomes. For non-targeted liposomes the spleen uptake at 4 hours was 33.9 ± 29.4% ID/g, and at 24 hours it reached the value of 82.5 ± 49.1% ID/g. Liver had the second highest normal organ uptake. Four hours after

administration, 9.1 ± 0.4% ID/g of immunoliposomes and 5.0 ± 1.7% ID/g of plain zwitterionic liposomes were observed in the liver. After 24 hours, the liver uptake increased to 14.1 ± 2.2% ID/g and 11.1 ± 2.3% ID/g for immunoliposomes and plain non-targeted liposomes, respectively. Kidney uptake was insignificant.

Biodistributions of plain zwitterionic liposomes in mice with and without tumor had no significantly different uptake by the spleen and liver.

Biodistributions of large cationic liposomes in tumor bearing mice

Large cationic liposomes demonstrated a tumor uptake pattern similar to zwitterionic liposomes (Figures 5A and 5B). Four hours after IP administration, tumor uptake was 21.3 ± 19.5%ID/g for cationic immunoliposomes, and 7.1 ± 2.5% ID/g for plain cationic liposomes; 24 hours after administration, the difference in tumor localization between immunoliposomes (21.7 ± 14.3% ID/g) and plain liposomes (18.6 ± 12.9% ID/g) was similar. Spleen uptake increased with time and 24 hours post-injection it reached the value of 148.7 ± 67.2% ID/g and 161.5 ± 104.0% ID/g for cationic immunoliposomes and non-targeted liposomes, respectively. Liver uptake, 4 hours post-injection, was 12.9 ± 11.3% ID/g for immunoliposomes and 10.0 ± 6.5% ID/g for plain non-targeted liposomes. Twenty-four hours later, it further increased to 21.4 ± 7.8% ID/g and 16.9 ± 7.2% ID/g for cationic imunoliposomes and plain liposomes, respectively. Kidney uptake was not significant. Blood uptake was low.

The biodistributions of plain cationic liposomes were similar in tumor bearing and tumor free mice, except for the spleen uptake that was significantly higher in the latter.

Blood uptake for all types of liposomes was between 2.7-8.0% ID/g at 4 hours and dropped to below 0.8% ID/g at 24 hours. Liver and spleen uptake of the cationic radioimmunoliposomes was greater than the corresponding values for zwitterionic immunoliposomes. Both immuno-liposomal compositions showed similar tumor uptake 4 hours after administration.

Imaging of liposomes in vivo

The distribution of ^{111}In-DTPA entrapping liposomes in mice after IP administration was imaged using a planar gamma-camera (Figure 6). No radioactivity into the circulation was observed, as is shown by the absence of radiation intensity in the cardiac region. The images suggest that liposomes are retained intact in the peritoneal region, since the native distribution of free ^{111}In-DTPA was not observed.

Fluorescence imaging of liposomes in the peritoneal cavity

To verify the presence of intact liposomes in the peritoneal cavity at later times after administration, large PEGylated liposomes with an encapsulated fluorophore (calcein), at self-quenching concentrations, were injected intraperitoneally in mice. Six hours later, the animals were sacrificed, the abdominal cavity was exposed and the peritoneal membrane was removed. To

detect any intact liposomes in the peritoneal cavity, Triton-X 100 was added to disrupt the intact structures, release calcein from the liposomes, relax self-quenching, and thereby increase the fluorescence intensity. The fluorescence images of the peritoneal cavities of mice are shown in Figures 7A and 7B for animals that were injected with zwitterionic (Figure 7A(i)) and cationic liposomes (Figure 7B(i)), respectively, before the addition of Triton-X 100. After addition of the lipid solubilizer, dramatic increase of fluorescence in the peritoneal fluid was observed for both animals, indicating that 6 hours after IP administration of liposomes, there are still intact liposomes in the peritoneal fluid (Figures 7A(ii) and 7B(ii)).

Mice that were administered fluorescent liposomes were also imaged 48 hours post-injection (data not shown). Intact zwitterionic and cationic liposomes were observed only in the mesentery, as verified by enhancement of the fluorescence intensity after Triton-X 100 addition.

DISCUSSION

Disseminated micrometastatic disease is usually incurable. Peritoneal dissemination is frequent in advanced colorectal and gynecologic cancers. Intraperitoneal administration of therapeutics for targeting peritoneal micrometastatic disease has the advantage of direct tumor access and may allow high tumor accumulation of therapeutics to be achieved before uptake levels in normal organs becomes a limiting factor. Also, because the onset of tumor vasculature development usually starts after a certain tumor size is reached, this route of administration is optimal for therapy of intraperitoneal micrometastases, which will not have developed vasculature.

Towards this goal, we developed large radioimmunoliposomes and studied their potential to target tumors in the peritoneal cavity. We use the term radioimmunoliposomes to define the liposomal structures that contain encapsulated radionuclides and, are conjugated, on their membrane, with tumor-targeting antibodies. In principle, radioimmunoliposomes have the potential to combine the targeting advantages of radioimmunotherapy, namely (a) specific tumor targeting, (b) enhanced tumor irradiation, and (c) minimal normal organ toxicity, with the delivery characteristics of liposomes, which include (a) vast internal volume for encapsulation of radioisotopes, and (b) considerable surface area for multivalent targeting-ligand conjugation. Over the last years, steric stabilization of liposomes *(11)* has resulted in reduction of their uptake and catabolism by the reticuloendothelial system, and, thus, has enabled their application in drug delivery. Liposomal encapsulation alters the

pharmacokinetics of IP administered agents which are cleared rapidly from the peritoneum through peritoneal membrane absorption, but, instead, follow the slower clearance of liposomes through lymphatic drainage.

Large zwitterionic and cationic PEGylated liposomes (650 nm in diameter) were prepared and characterized for content leakage (calcein release) and size (DLS) over time. Liposomes were stable during a period of 20 days in ascites fluid and in media (1-10% serum) at 37^{o}C. The small increase in the average liposome diameter over time could possibly be due to fusion among liposomes that is driven by the tendency to decrease the bending energy of the bilayer membrane.

Liposomes were immunolabeled with the antiHER2/neu monoclonal antibody Trastuzumab with an efficiency of 65-95 antibodies per zwitterionic liposome and 95-130 antibodies per cationic liposome. Enhanced specific binding of immunoliposomes to the HER2/neu antigen receptor of the human ovarian carcinoma cell line SKOV3 was demonstrated by flow cytometry. Non specific binding was not detected for the zwitterionic liposomes. Cationic immunoliposomes associated with cells to some extent even after blocking of the antigen receptor, probably due to electrostatic interactions between the positively charged liposomal membrane and the locally negatively charged cell membrane *(21)*. Similarly, non-specific binding was also observed for the plain non-targeted cationic liposomes. The increased binding of cationic immunoliposomes (mean shift = 74) compared to zwitterionic immunoliposomes (mean shift = 59) could be explained not only by the non-

specific electrostatic interactions of the first, but also by the higher surface-density of antibodies on cationic liposomes.

Quantification of binding and internalization of liposomes to SKOV3 cells was determined using liposomes with encapsulated ^{111}In-DTPA. Both zwitterionic and cationic immunoliposomes rapidly bound and internalized into SKOV3 ovarian carcinoma tumor cells. After 4 hours of incubation, the fraction of internalized activity was >55% and >66% of the total cell-associated activity for zwitterionic and cationic immunoliposomes, respectively. Saturation of the internalization mechanism, after 4 hours of incubation, was observed only for zwitterionic immunoliposomes and not for cationic immunoliposomes. Since the cationic immunoliposome-cell interaction includes a substantial non-specific component, we speculate that this non-specific and possibly non-saturable component is also operative for internalization. Total cell-associated activity of cationic immunoliposomes was more extensive, 10-fold more, than zwitterionic immunoliposomes, and it increased throughout the period of 24 hours.

Similar binding and internalization curves for both types of immunoliposomes were obtained when liposomes with higher surface-density of conjugated antibodies were used (data not shown). Minimal cell association *in vitro* was observed with plain non-targeted zwitterionic and cationic liposomes.

Spleen and liver uptake are considered significant features of liposomal biodistribution, *in vivo*. To effectively target and irradiate peritoneally disseminated micrometastases, we developed large radioimmunoliposomes

that can rapidly target tumors after IP administration, and studied the kinetics of their accumulation to the spleen and liver. Because the maximum uptake by those organs is reached a few hours after administration, to minimize the toxicity effects to the spleen and liver, we propose liposomal entrapment of radionuclides with half-lives shorter than this time frame. Also, intravenous pre-injection of unlabeled plain liposomes could be used to saturate these sites *(22)*. It is of major importance, however, that the large liposomes we studied showed no significant blood and kidney uptake. In addition, due to the high number of radionuclei encapsulated per liposome, high radiation dose per liposome can be delivered at the tumor site.

Encapsulated ^{111}In-DTPA was used that allows for animal imaging and quantitation of the radioactivity of the excised organs. The highest normal organ accumulation was observed in the liver and spleen. The maximum uptake was observed 8 hours post-injection for both liposomal compositions. The gamma camera images of the animals suggested peritoneal retention of liposomes and did not show detectable increase in the blood pool concentration or in the kidney uptake. Peritoneal retention of intact liposomes was directly confirmed, 6 hours after IP administration, by fluorescence imaging and relief of self-quenching of calcein encapsulating liposomes. Fourty-eight hours later, only a few intact liposomes were detected in the mesenteric region by the same method.

The tumor targeting efficiency of immunoliposomes *in vivo* showed that immunolabeling of liposomes results in enhancement of tumor targeting at

short times (4 hours post-injection), demonstrated by a 6.5-fold increase in tumor uptake between zwitterionic immunoliposomes and zwitterionic plain liposomes, and a 3-fold increase for the cationic composition. At later times (24 hours post injection), the difference in tumor uptake between immunoliposomes and plain liposomes was less significant. Cationic immunoliposomes showed higher mean tumor uptake than zwitterionic immunoliposomes, but this result may be due to the moderately different numbers of conjugated antibodies per liposome between the two types of immunoliposomes. The tumor uptake values for plain liposomes were significant, and were in contrast to their minimal cell binding that was observed *in vitro*. Tumor uptake of plain cationic liposomes was higher compared to plain zwitterionic liposomes, which was in accordance with the flow cytometry observations.

The SKOV3 ovarian carcinoma animal model and the IP administered antiHER2/neu large radioimmunoliposomes were selected as a proof of principle for effective targeting of tumors in the peritoneal cavity for potential radionuclide therapy of micrometastatic dissemination. *In vitro* studies showed that after cell binding large radioimmunoliposomes were internalized to a significant extent. Immunolabeled liposomes showed rapid and increased tumor uptake before the maximum liver concentrations were reached. Because of those two characteristics of the radioimmunoliposomes studied, we propose their potential application in IP radiotherapy of micrometastases with entrapped emitters of short-range and short half-life. Alpha-particle

emitters might be the most appropriate, since the range of alpha-particles (50-80 μm) is relatively short and should not cause significant abdominal radiotoxicity due to the prolonged retention of liposomes in the peritoneal cavity. The alpha-emitters such as ^{211}At ($t_{1/2}$=7.21 hours) or ^{213}Bi ($t_{1/2}$=45 min) are promising candidates, because they will have significantly decayed by the time the maximum normal organ uptake will be achieved.

Conclusion

We have engineered large antiHER2/neu radioimmunoliposomes that can rapidly and effectively target intraperitoneal tumors in an ovarian carcinoma animal model. Large liposomes are intact in the peritoneal cavity for hours after IP administration, and accumulate to normal organs (liver and spleen) with relatively low rates. *In vitro*, large radioimmunoliposomes bind and internalize into SKOV3 cells to a significant extent.

Large radioimmunoliposomes, with encapsulated short-half life, short-range emitters, are potential agents for the therapy of (or prophylaxis against) peritoneal micrometastatic disease.

Acknowledgements

We thank Prof. Iwao Teraoka (Polytechnic University) for use of the DLS apparatus. This study was supported by Concept and IDEA awards DAMD170010657 and DAMD170310755, respectively from the U.S. Army Medical Research and Materiel Command, grant R01 CA55349 from the National Institutes of Health, the Doris Duke Charitable Foundation, the Experimental Therapeutics Center, the Goodwin Commonwealth Foundation for Cancer Research, and the Dr. Frederick E.G. Valergakis Graduate Research Grant of the Hellenic University Club of New York.

References

1. Buijs WCAM, Tibben JG, Boerman OC, et al. Dosimetric analysis of chimeric monoclonal antibody cMOv18 IgG in ovarian carcinoma patients after intraperitoneal and intravenous administration. *Eur J Nucl Med*. 1998;25:1552-1561.
2. Borchardt P, Yuan R, Miederer M, et al. Targeted actinium-225 in vivo generators for therapy of ovarian cancer. *Cancer Res*. 2003;63:5084.
3. Li C-Y, Shan S, Huang Q, et al. Initial Stages of Tumor Cell-Induced Angiogenesis: Evaluation Via Skin Window Chambers in Rodent Models. *J Natl Cancer Inst*. 2000;92:143-147.
4. Cullis PR, DeKruijff B. Lipid polymorphism and the functional role of lipids in biological membranes. *Biochim Biophys Acta*. 1979;559:399-420.
5. Epenetos A, Munro A, Stewart S, et al. Antibody-guided irradiation of advanced ovarian cancer with intraperitoneally administered radiolabeled monoclonal antibodies. *J Clin Oncol*. 1987;5:1890-1899.
6. Crippa F, Bolis G, Seregni E, et al. Single-dose intraperitoneal radioimmunotherapy with the murine monoclonal antibody I-131 MOv18: Clinical results in patients with minimal residual disease of ovarian cancer. *Eur J Cancer*. 1995;31:686-690.
7. Meredith R, Partridge E, Alvarez R, et al. Intraperitoneal radioimmunotherapy of ovarian cancer with Lutetium-177-CC49. *J Nucl Med*. 1996;37:1491.

8. Delgado G, Potkul R, Treat J, et al. A phase I/II study of intraperitoneally administered doxorubicin entrapped. *Am J of Obs Gyn*. 1989;160:812.

9. Verschraegen C, Kumagai S, Davidson R, et al. Phase I clinical and pharmacological study of intraperitoneal cis-bis-neodecanoato(trans- R, R-1, 2-diaminocyclohexane)-platinum II entrapped in multilamellar liposome vesicles. *J Cancer Res Clin Oncol*. 2003;129:549-555.

10. Kirpotin DB, Park JW, Hong SK, et al. Sterically stabilized anti-HER2 immunoliposomes: design and targeting to human breast cancer cells *in vitro*. *Biochemistry*. 1997;36:66-75.

11. Sapra P, Allen TM. Ligand-targeted liposomal anticancer drugs. *Prog Lipid Res*. 2003;42:439-462.

12. Junghans RP, Sgouros G, Scheinberg DA. Andibody-based immunotherapies for cancer. In: Chabner BA, Longo DL, editors. Cancer Chemotherapy and Biotherapy. Philadelphia: Lippincott-Raven Publishers; 1996. p 678.

13. Nikula TK, Bocchia M, Curcio MJ, et al. Impact of the high tyrosine fraction in complementarity determining regions: measured and predicted effects of radioiodination on IgG immunoreactivity. *Mol Immun*. 1995;32:865-872.

14. Castile JD, Taylor KMG. Factors affecting the size distribution of liposomes produced by freeze-thaw extrusion. *Int J Pharm*. 1999;188:87-95.

15. Hwang KJ, Merriam JE, Beaumier PL, et al. Encapsulation, with high efficiency, of radioactive metal ions in liposomes. *Biochim Biophys Acta*. 1982;716:101-109.

16. Stensrud G, Redford K, Smistad G, et al. Effects of gamma irradiation on solid and lyophilised phospholipids. *Rad Phys Chem*. 1999;56:611-622.

17. McIntyre JC, Sleight RG. Fluorescence assay for phospholipid membrane asymmetry. *Biochemistry*. 1991;30:11819-11827.

18. Provencher SW. A constrained regularization method for inverting data represented by linear algebraic or integral equations. *Comput Phys Commun*. 1982;27:213-227.

19. Teraoka I. *Polymer Solutions: An Introduction to Physical Properties*. New York, NY: John Wiley & Sons; 2002. 188-191 p.

20. Lasic DD. *Liposomes from Physics to Applications*. Amsterdam: Elsevier; 1993. 555 p.

21. Devaux PF. Protein Involvement in Transmembrane Lipid Asymmetry. *Ann Rev Biophys Biomolec Struct*. 1992;21:417-439.

22. Drummond DD, Meyer O, Hong K, et al. Optimizing liposomes for delivery of chemotherapeutic agents to solid tumors. *Pharmacol Rev*. 1999;51:691-743.

Table 1

Retention of entrapped contents by zwitterionic and cationic liposomes in media (1-10% serum) at 37^{o}C for 30 days.

Time [days]	Large Zwitterionic Liposomes Δq x 100*			Large Cationic Liposomes Δq x 100*		
	1% serum	5% serum	10% serum	1% serum	5% serum	10% serum
1	0± 9	0± 7	0± 6	0± 7	0± 7	0± 6
2	17± 9	14± 6	6± 6	2± 6	-2± 6	2± 5
3	21± 8	14± 6	8± 7	15± 7	10± 7	15± 7
14	22±10	6± 6	0± 6	32± 6	6± 6	5± 6
30	21± 9	-1± 6	-9±6	39± 6	0± 7	-5± 6

* Fractional fluorescence self-quenching decrease due to calcein leakage from PEGylated liposomes over time ($\Delta q_{day\_x}=(q_{day\_1}-q_{day\_x})/ q_{day\_1}$). After the first 24 hours a maximum of 17% in self-quenching decrease was measured for all liposomes (possibly due to differences in osmotic pressure across the liposomal membrane). Beyond this point all liposomes were generally stable for over 30 days. The uncertainties correspond to standard errors of repeated measurements.

Table 2

Retention of entrapped contents by zwitterionic and cationic liposomes in ascites fluid at 37^{o}C for 30 days.

Time [days]	Zwitterionic Liposomes	Cationic Liposomes
	$\Delta q \times 100$*	
1	0±9	0±12
2	0±9	-9±10
3	0±8	-4±11
10	19±8	1±10
15	21±7	0±9
20	47±7	26±9
30	69±7	52±9

* Fractional fluorescence self-quenching decrease due to calcein leakage from PEGylated liposomes over time ($\Delta q_{day\_x}=(q_{day\_1}-q_{day\_x})/ q_{day\_1}$). After the first 15 days a maximum of 21% in self-quenching decrease was measured for all liposomes. The uncertainties correspond to standard errors of repeated measurements.

LEGENDS

Figure 1. Binding of rhodamine-labeled plain liposomes and immunoliposomes to SKOV3 cells. Thin solid line: SKOV3 cells; Shaded gray: fluorescence of liposomes bound to SKOV3 cells with blocked HER2/neu antigen receptors; Thick solid line: fluorescence of liposomes bound to unblocked SKOV3 cells. (A) Zwitterionic immunoliposomes, (B) Zwitterionic plain liposomes, (C) Cationic immunoliposomes, (D) Cationic plain liposomes, (E) Control. Shaded gray: Binding of TRITC-labeled Rituximab to SKOV3 cells (irrelevant antibody). Shaded black: Binding of TRIC-labeled trastuzumab to SKOV3 cells (relevant antibody).

Figure 2. Cell binding and internalization of liposomes. ^{111}In-labeled liposomes were added to ice cold, blocked SKOV3 cells, 10^6cells/ml. Cells were transferred to a 37^{o}C incubator and were sampled at 0, 0.5, 1, 2, 4, and 24 hours. Samples were washed and surface bound liposomes were removed by an acidic stripping buffer at room temperature. The activities of supernatants and pellets were then quantified in a gamma-counter. (A) zwitterionic liposomes, (B) cationic liposomes. ● total cell-associated activity of immunoliposomes, ○ cell internalized activity of immunoliposomes, ▼total cell-associated activity of plain liposomes. The error bars correspond to standard deviations.

Figure 3. Biodistributions of i.p. administered ^{111}In-DTPA labeled zwitterionic liposomes (A), cationic liposomes (B), and free ^{111}In-DTPA (C). Mice (n = 7) were

sacrificed at 1, 4, 8, and 24 hours post-injection, and blood, heart (blotted to remove blood), lungs, liver, spleen, stomach, intestines, kidneys, bone (with marrow), and muscle were sampled, weighted, and then counted with a gamma-counter. The %I.D./g for each sample was then determined. The error bars correspond to standard deviations.

Figure 4. Biodistributions of IP administered ^{111}In-DTPA labeled zwitterionic liposomes. Female athymic nude mice bearing 14-day-old IP xenographs of SKOV3 cells were sacrificed at 4 (open bars) and 24 (shaded bars) hours after administration of immunoliposomes (A) or plain liposomes (B) (n = 3-5), and blood, heart, lungs, liver, spleen, stomach, intestines, kidneys, bone, muscle, and tumor were sampled, weighted, and then counted with a gamma-counter. The %I.D./gr for each sample was then determined. The error bars correspond to standard deviations.

Figure 5. Biodistributions of IP administered ^{111}In-DTPA labeled cationic liposomes. Female athymic nude mice bearing 14-day-old IP xenographs of SKOV3 cells were sacrificed at 4 (open bars) and 24 (shaded bars) hours after administration of immunoliposomes (A) or plain liposomes (B) (n = 4), and blood, heart, lungs, liver, spleen, stomach, intestines, kidneys, bone, muscle, and tumor were sampled, weighted, and then counted with a gamma-counter. The %I.D./gr for each sample was then determined. The error bars correspond to standard deviations.

Figure 6. Planar gamma-camera images of mice after IP administration of ^{111}In-DTPA labeled zwitterionic liposomes. Animals were imaged 1, 4, 8, and 24 hours post-injection.

Figure 7. Detection of intact liposomes in the peritoneum using fluorescence imaging of IP administered calcein-containing zwitterionic (A) and cationic (B) liposomes. Mice were sacrificed 6 hours after administration of cationic liposomes with entrapped self-quenching concentrations of calcein. Addition of Triton-X 100 disrupts the intact liposomes, calcein is released from the liposomes, and the fluorescence signal is increased due to relief of self-quenching. (i) Fluorescence image of the peritoneal cavity before addition of Triton-X 100. (ii) After detergent addition.

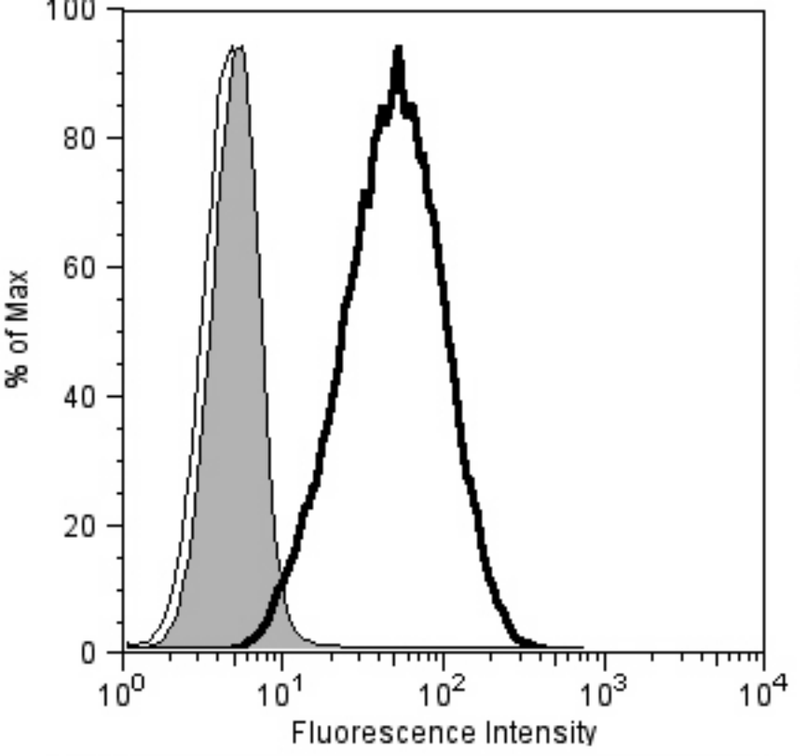
% of Max
Fluorescence Intensity

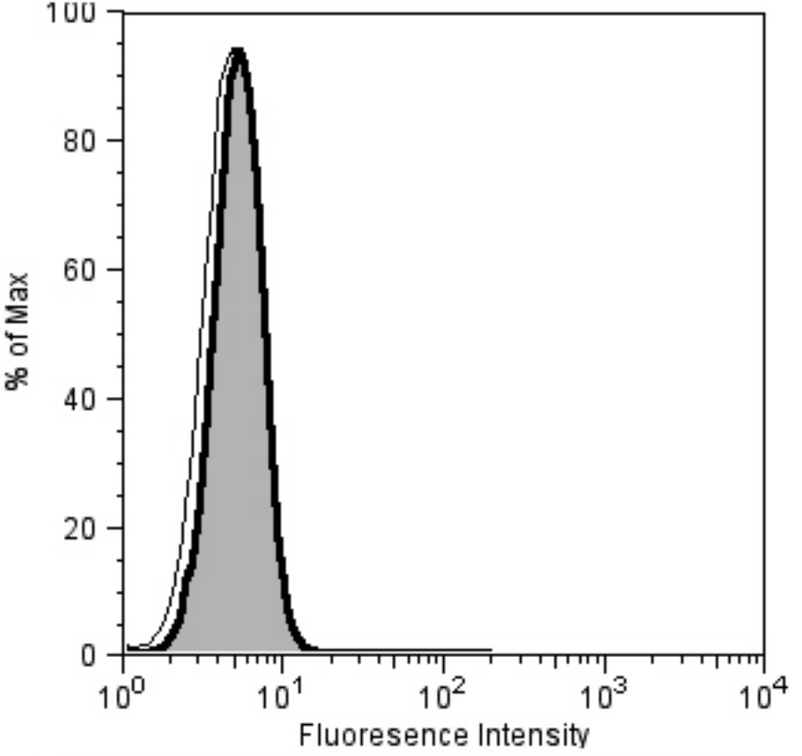
% of Max
Fluoresence Intensity

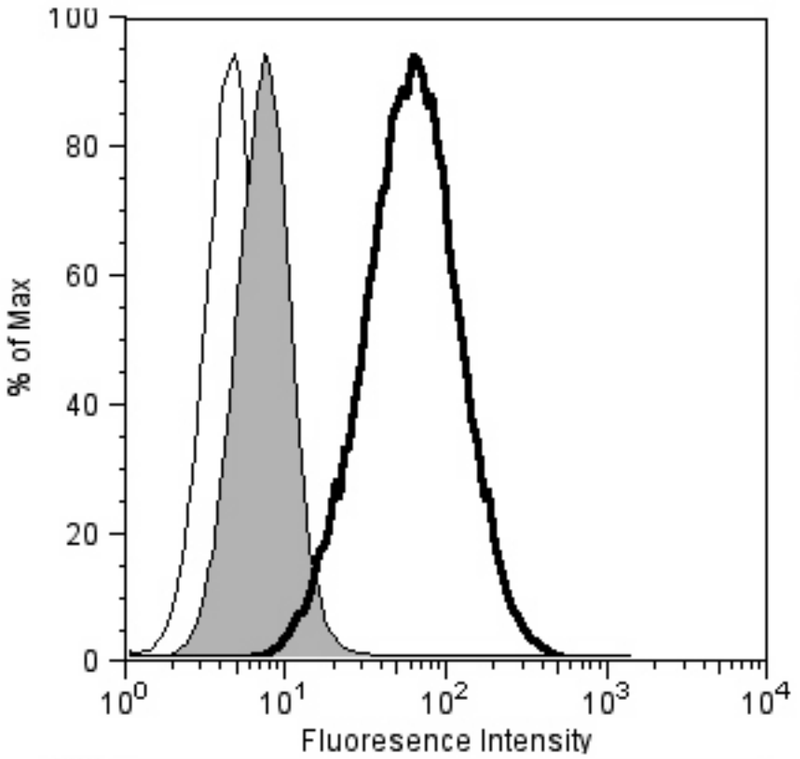
% of Max
Fluoresence Intensity

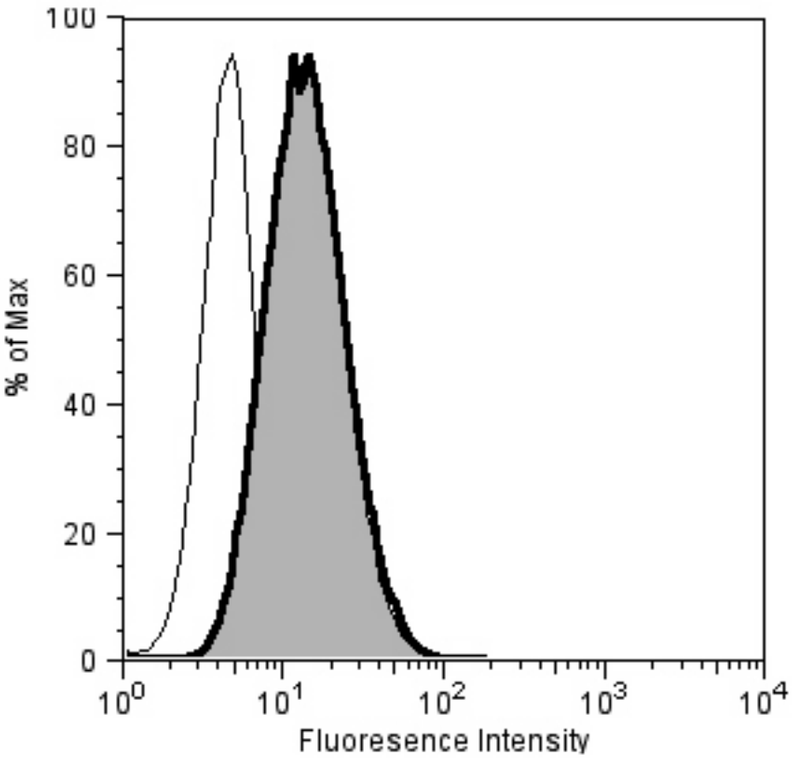
% of Max
Fluoresence Intensity

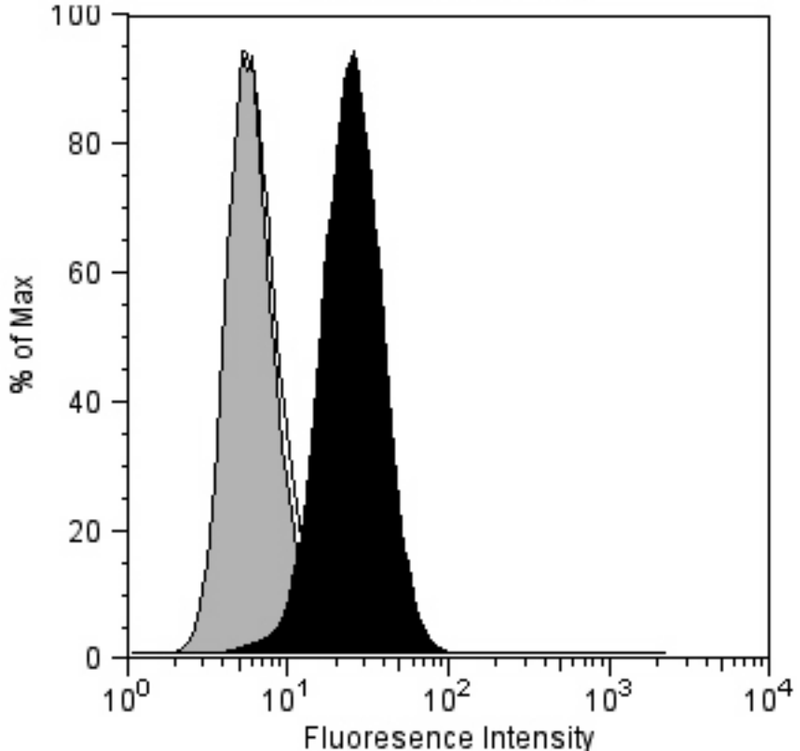
% of Max
Fluoresence Intensity

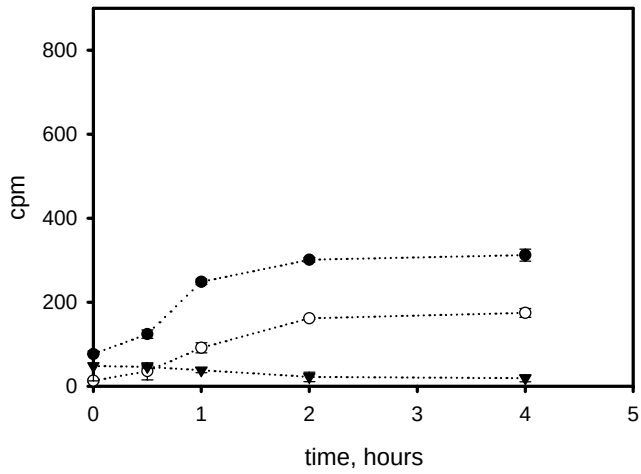

Figure 2A

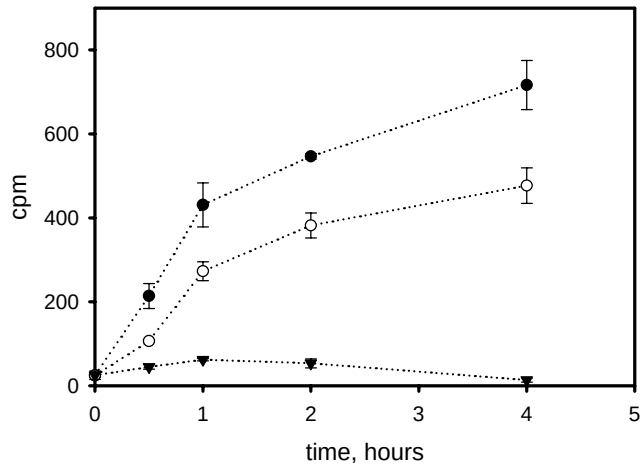

Figure 2B

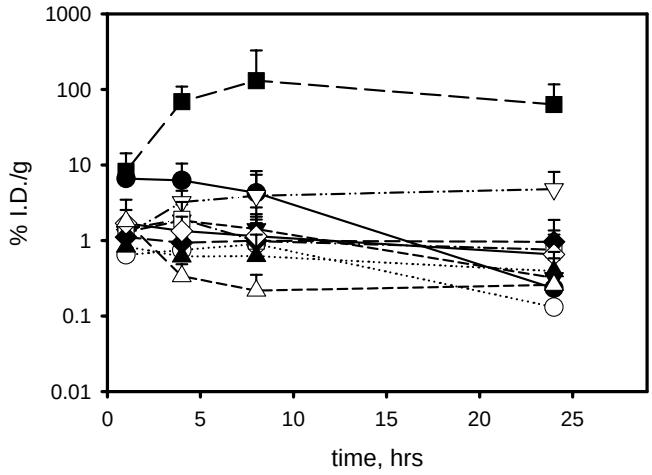

Figure 3A

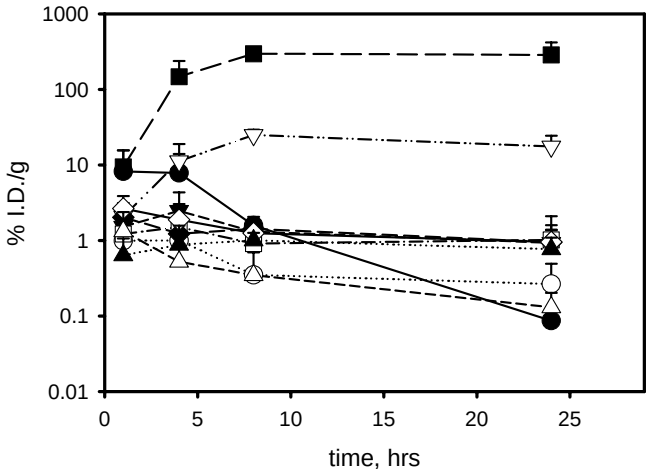

Figure 3B

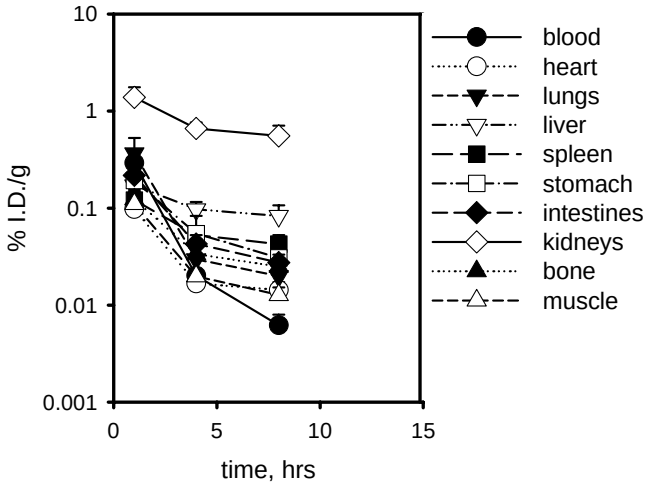
10
1
0.1
0.01
0.001
% I.D./g
0
5
10
15
time, hrs
blood
heart
lungs
liver
spleen
stomach
intestines
kidneys
bone
muscle

Figure 3C

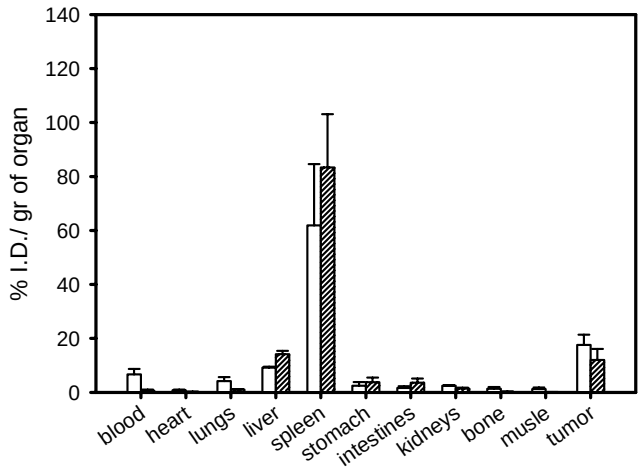
140
120
100
80
60
40
20
0
% I.D./ gr of organ
blood
heart
lungs
liver
spleen
stomach
intestines
kidneys
bone
musle
tumor

Figure 4A

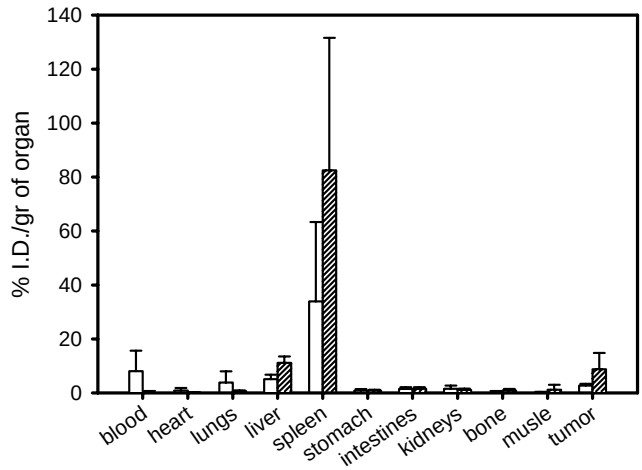
140
120
100
80
60
40
20
0
% I.D./gr of organ
blood
heart
lungs
liver
spleen
stomach
intestines
kidneys
bone
musle
tumor

Figure 4B

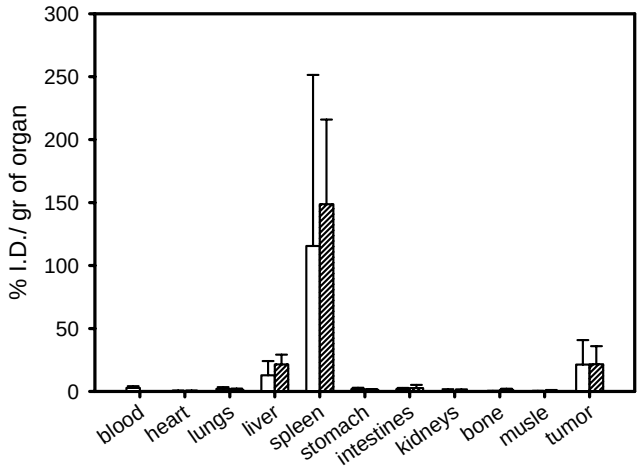
300
250
200
150
100
50
0
% I.D./ gr of organ
blood
heart
lungs
liver
spleen
stomach
intestines
kidneys
bone
musle
tumor

Figure 5A

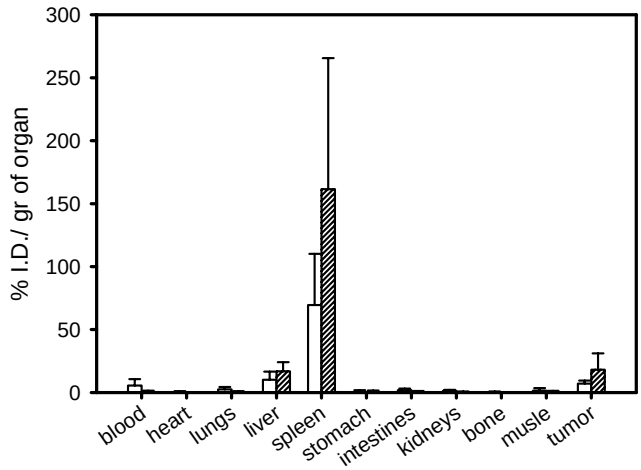
300
250
200
150
100
50
0
% I.D./ gr of organ
blood
heart
lungs
liver
spleen
stomach
intestines
kidneys
bone
musle
tumor

Figure 5B

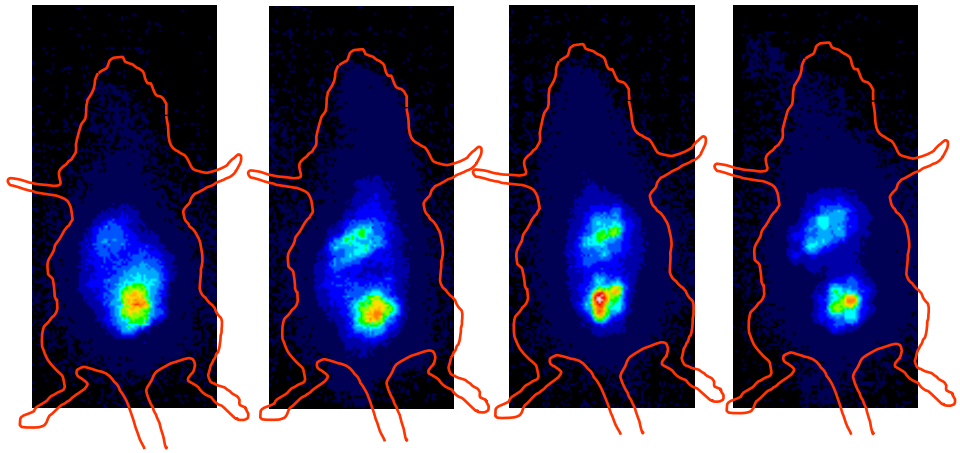

Figure 6

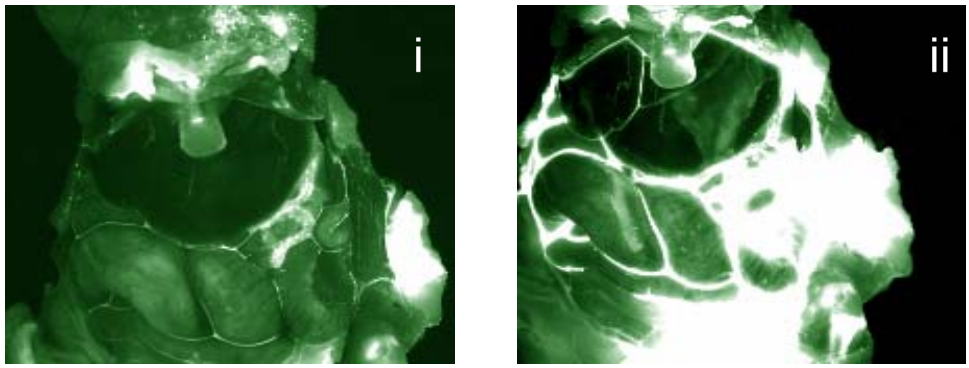

Figure 7A

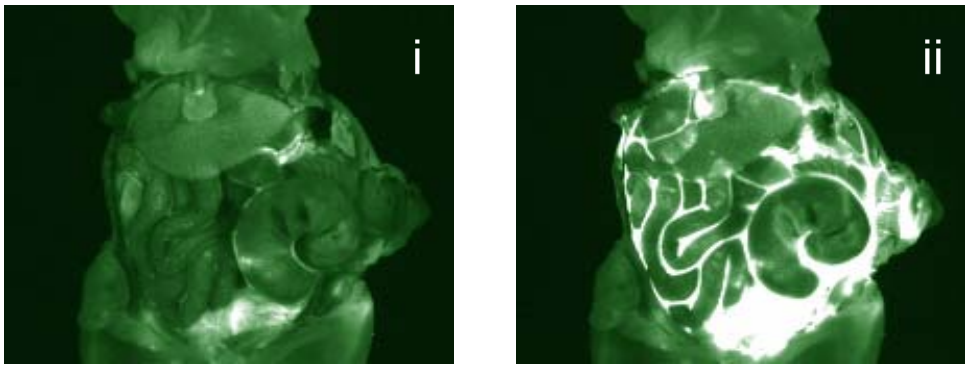

Figure 7B

Enhanced Retention of the α-particle Emitting Daughters of Actinium-225 by Engineered Liposomal Carriers for Targeted Therapy of Micrometastatic Cancer

Stavroula Sofou, PhD[1,†]; Barry Kappel, B.A.[1]; Jaspreet S. Jaggi[1]; Michael R. McDevitt, PhD[1]; David A. Scheinberg, MD, PhD[1]; and George Sgouros, PhD[2].

Molecular Pharmacology and Chemistry (1), Memorial Sloan-Kettering Cancer Center, 1275 York Ave, New York, NY 10021

Department of Radiology (2), Division of Nuclear Medicine, Johns Hopkins Medicine, 220 Ross Research Building, 720 Rutland Ave, Baltimore, MD 21205

[†] Present address: Department of Chemical and Biological Engineering, Polytechnic University, 6 MetroTech Center, Brooklyn, NY 11201

Work supported by the USAMRMC Concept Award DAMD170010657, USAMRMC IDEA Award DAMD170310755, NIH R01 CA55349, the Experimental Therapeutics Center, and the Goodwin Commonwealth Foundation for Cancer Research. D.A.S. is a Doris Duke Distinguished Science Professor. S.S. is the recipient of Dr. Frederick E.G. Valergakis Graduate Research Grant of the Hellenic University Club of New York

Running title: 'Multivesicular Liposomes for alpha-therapy'

Abstract

Targeted α-particle emitters hold great promise as therapeutics for micrometastatic disease. Because of their high energy deposition, only 1 to 3 α-particle traversals through the cell nucleus are required for cell killing. In addition, the short range of α-particles (50-100 microns) is consistent with the dimensions of micrometastases, allowing for minimal normal-tissue irradiation. Actinium-225 decays with a 10-day half-life and generates three α-particle emitting daughters, rendering ^{225}Ac an attractive candidate for α-therapy.

Retention of these daughters at the target site increases efficacy; escape and distribution throughout the body increases toxicity. Antibodies with conjugated ^{225}Ac cannot retain any of the daughters. Liposomal encapsulation of ^{225}Ac showed that daughter retention was liposome-size dependent, but was lower than expected, due to binding of ^{225}Ac to the phospholipid membrane. To increase daughter retention, ^{225}Ac was passively entrapped in multivesicular liposomes (MUVEL). MUVELs are large liposomes with entrapped smaller lipid-vesicles, containing ^{225}Ac. This strategy provides confinement of entrapped ^{225}Ac within the region of the liposomal core, away from the outer liposomal membrane. PEGylated MUVELs yielded 98% ^{225}Ac retention, and 18% retention of the last daughter ^{213}Bi. MUVELs were then conjugated to an anti-HER2/neu antibody, and exhibited strong binding to and significant internalization (83%) by ovarian carcinoma SKOV3 cells. Upon intraperitoneal administration of ^{225}Ac-containing MUVELs to animals with intraperitoneally disseminated tumors, significant tumor uptake of ^{225}Ac and its daughters was detected.

This work demonstrates that radioimmunolabeled-MUVELs could make it possible to retain the high potency of ^{225}Ac while reducing its toxicity associated with untargeted daughter emissions.

Introduction

Targeted α-particle emitters hold great promise as therapeutic agents for micrometastases (1). Alpha-particles are highly potent cytotoxic agents, potentially capable of tumor-cell kill without limiting morbidity. The increased effectiveness of α-particles is due to the amount of energy deposited per unit distance traveled (linear energy transfer, or LET), which is of the order of approximately 80 keV/μm. Cell survival studies have shown that α-particle–induced killing is independent of oxygenation state or cell-cycle during irradiation and that as few as 1–3 tracks across the nucleus may result in cell death (2-4). In addition, the 50- to 100-μm range of α-particles is consistent with the dimensions of micrometastatic disseminated disease, allowing for localized irradiation of target cells with minimal normal-cell irradiation. Actinium-225 is an α-particle emitter with increased cell killing efficacy (5-7), because each actinium-225 decay ($t_{1/2}$=10 d) generates three α-particle emitting daughters (^{221}Fr ($t_{1/2}$=4.9 min), ^{217}At ($t_{1/2}$=32.3 ms), ^{213}Bi ($t_{1/2}$=45.59 min)), and a total of 4 α -particles per decay (Figure 1A). Thus, ^{225}Ac is an attractive candidate for α-particle emitter therapy.

However, the optimal increase in cell killing efficacy of ^{225}Ac will occur if all α-emissions occur at the tumor site; otherwise, toxicity may be potentially increased. This is a fundamental difficulty if antibodies or other molecular ligands are to be used as the cell targeting vehicle, since the chemical bond holding the ^{225}Ac atom to the delivery molecule will be broken after decay of ^{225}Ac. This will leave the first daughter in the decay-chain free to distribute throughout the body where it and the resulting daughters will decay and increase toxicity. Thus, confinement of these intermediates (radioactive daughters) to the targeted tumor is desirable.

Liposomes have been previously considered for diagnostic and therapeutic delivery of radionuclides (8-12). We have previously investigated encapsulation of ^{225}Ac in liposomes as a

means of retaining daughter α-particle emissions at the site of liposomal delivery (13). Because of their high kinetic energy, α-particle emissions will escape the liposomal phospholipid membrane to irradiate the targeted cells located at radii ranging from 50 to 100 microns. Similarly, a daughter atom, that is produced after emission of an α-particle, experiences a recoil of 80 to 100 nm. During their recoil trajectory, the newly produced daughter atoms can also penetrate the phospholipid membranes. However, the newly produced daughter atoms are charged, so after loosing their recoil energy, daughter atoms cannot diffuse freely across the hydrophobic compartment of the phospholipid bilayer. As a result, if the end-point of a daughter's recoil trajectory is located within a liposome, the lipid membrane will inhibit free diffusion of the daughter atoms, thereby retaining them at the site of liposome delivery. The probability of daughter retention is greater for larger liposomes assuming homogeneous distribution of the parent radionuclides within the liposome aqueous compartment (Figure 1B). Consequently, retention of daughters is liposome size dependent. Theoretical calculations predicted negligible, <0.001 % (last) daughter retention for 100 nm diameter liposomes and more than 50% retention (of the last daughter) for liposomes larger then 650 nm (in diameter). The measured last daughter retention (11 % decreasing to 4% after 30 days) of 650 nm diameter liposomes was not consistent with the theoretical prediction, however. This was shown to be caused, in part, due to binding of ^{225}Ac to the phospholipid membrane (13). Actinium-225 localization to the liposomal membrane increases daughter loss after nuclear recoil, compared to daughter loss from uniformly distributed ^{225}Ac atoms within the liposomal aqueous phase. The direction of daughter recoil is random, thus daughter retention by liposomes is a function of the position of the parent nucleus: the closer the nuclear recoil occurs to the liposomal membrane the lower the probability that the newly formed daughter will be retained in the liposome (Figure 1B). In this work we describe and characterize a construct designed to overcome this problem.

To increase daughter retention, ^{225}Ac was passively entrapped in MUltiVEsicular Liposomes (MUVELs). MUVELs are large liposomes with entrapped smaller lipid-vesicles. Actinium-225 was contained in the small vesicles only. This strategy provides (a) confinement of entrapped ^{225}Ac within the aqueous compartment of the large liposomes where the small vesicles are contained, and, thus, away from the large liposome membrane, and (b) results in decreased radionuclide partition to the external membrane (large liposome membrane), due to increased internal membrane owed to the encapsulated small vesicles.

MUVELs were prepared and characterized over time for size and content leakage (^{225}Ac, ^{213}Bi). Minimal loss of ^{225}Ac from MUVELs was detected, and the α-particle delivery was significantly increased. Immunolabeled MUVELs were then evaluated for targeted delivery of ^{225}Ac to disseminated micrometastatic tumors in the peritoneal cavity of ovarian carcinoma bearing mice. Advanced ovarian cancer usually metastasizes in the peritoneal surface. We followed intraperitoneal (IP) administration of the ^{225}Ac liposomal carriers, because the particular strategy has the advantage of direct tumor access (14-16), and may allow for high tumor accumulation of therapeutics even at micrometastatic sites that do not have developed vasculature (17).

To achieve specific tumor targeting and internalization, PEGylated MUVELs were labeled with the monoclonal antibody trastuzumab that targets HER2/neu which is overexpressed on the surface of ovarian carcinoma cells (SKOV3). Such radioimmunoliposomes should combine the following beneficial features: (a) targeting efficacy and specificity due to the surface-conjugated tumor-specific antibodies (18, 19); (b) long retention times in the peritoneal cavity (20, 21), due to large liposome sizes; (c) a radiation dose range tailored to micrometastases; and (d) minimal irradiation of the surrounding healthy tissues due to the α-particles' comparatively short range.

MATERIALS AND METHODS

Reagents

The lipids 1,2-Dimyristoyl-*sn*-Glycero-3-Phosphocholine (DMPC), 1,2-Diheneicosanoyl-*sn*-Glycero-3-Phosphocholine (21:0PC), 1,2-dipalmitoyl-sn-glycero-3-phosphoethanolamine-N-[methoxy(polyethyleneglycol)-2000] (ammonium salt) (PEG-labeled lipid), L-α-phosphatidylethanolamine-N-(lissamine rhodamine B sulfonyl) (egg) (rhodamine-PE), 1,2-distearoyl-*sn*-glycero-3-phosphoethanolamine-N-[maleimide (polyethylene glycol) 2000] (ammonium salt) (maleimide-PE) (purity >99%) were purchased from Avanti Polar Lipids (Alabaster, Al). Cholesterol, phosphate buffered saline (PBS), fluorexon (calcein), Sephadex G-50, diethylenetriaminepentaacetic acid (DTPA), 8-hydroxyquinoline (oxine), ascorbic acid, and Triton X-100 were purchased from Sigma-Aldrich (St. Louis, MO). p-isothiocyanatobenzyl-1,4,7,10-tetraazacyclododecane-1,4,7,10-tetraacetic acid (DOTA) was purchased from Macrocyclics (Dallas, TX). Traut's reagent (2-Iminothiolane-HCl) was purchased from Pierce (Rockford, IL). Actinium-225 was purchased from the Department of Energy, Oak Ridge National Laboratories (Oak Ridge, TN).

Liposome preparation

The protocol to make multivesicular liposomes is described, in detail, elsewhere (22). Briefly, to make small vesicles, mixtures of phosphatidyl choline (21:0PC), cholesterol (1:1 molar ratio), and PEG-labeled lipids (5.3 mole % of total lipid) in $CHCl_3$ were dried in a rotary evaporator. For ^{225}Ac passive entrapment, the lipids were resuspended in PBS containing chelated actinium complexes (^{225}Ac-DOTA, 3.7-37.0 MBq) and diethylenetriaminepentaacetic acid (DTPA). The lipid suspension was then annealed to 55^{o}C for 2 hours. Small vesicles were prepared by brief sonication (1-2 min) of the lipid suspension in a bath sonicator (Branson, Danbury, CT) at 70-80^{o}C until appearance of a clear solution. The vesicle suspension was then incubated for 15 minutes with externally added DTPA, and unentrapped contents were removed by size

exclusion chromatography (SEC) in a Sephadex G-50 (Aldrich, St. Louis, MO) packed 1x10 cm column, eluted with a sucrose isotonic phosphate buffer.

To make large multivesicular liposomes, mixtures of phosphatidyl choline (DMPC), cholesterol (2:1 molar ratio), maleimide-PEG- labeled lipids (1 mole % of total lipid) and PEG-labeled lipids (4.3 mole % of total lipid) in $CHCl_3$ were dried in a rotary evaporator. For passive entrapment of small vesicles, the lipids were resuspended in sucrose-PBS solution containing small vesicles (prepared as described above). The lipid suspension was then annealed to 40^{o}C for 2 hours. Multivesicular liposomes were prepared by the extrusion method. The lipid suspension was taken through twenty-one cycles of extrusion (LiposoFast, Avestin, Ontario, Canada) through two stacked polycarbonate filters (800 nm filter pore diameter), and then diluted in sucrose-free isosmotic PBS solution. Unentrapped small vesicles were removed by centrifugation, and the majority of multivesicular liposomes were collected in the pellet.

To make large shells, mixtures of phosphatidyl choline (DMPC), cholesterol (2:1 molar ratio), maleimide-PEG- labeled lipids (1 mole % of total lipid) and PEG-labeled lipids (4.3 mole % of total lipid) in $CHCl_3$ were prepared using the same protocol as for multivesicular liposomes, without encapsulating small vesicles.

Ascorbic acid (8 mmol/l) was coentrapped to minimize lipid oxidation due to radiation (23).

Liposome size distribution determination

Dynamic light scattering (DLS) of liposome suspensions was studied with an N4 Plus autocorrelator (Beckman-Coulter), equipped with a 632.8 nm He-Ne laser light source. Scattering was detected at 15.7^{o}, 23.0^{o}, 30.2^{o}, and 62.6^{o}. Particle size distributions at each angle were calculated from autocorrelation data analysis by CONTIN (24). The average

liposome size was calculated to be the y-intercept at zero angle of the measured average particle size values vs $\sin^2(\theta)$ (25). All buffer solutions used were filtered with 0.22 μm filters just prior to liposome preparation. The collection times for the autocorrelation data were 1-4 minutes.

Retention of entrapped contents by liposomes

As shown on Figure 1A, ^{225}Ac ($t_{1/2}$ = 10 d) decays to the following α-emitting radionuclides: ^{221}Fr, ^{217}At, and ^{213}Bi. The protocol to experimentally measure the retention of ^{225}Ac and its daughters by the liposomes is described, in detail, elsewhere (13). Briefly, the γ-emissions of ^{213}Bi were measured in liposome fractions, which were separated from the parent liposome population and the free radionuclides, at different times. Unentrapped radionuclides were separated by SEC (Sephadex G-50) 15 to 30 minutes after addition of DTPA, and the samples were counted using a Cobra γ-counter (Packard Instrument Co., Inc.). Under equilibrium conditions the decay rate of ^{213}Bi was used to determine the concentration of ^{225}Ac. Kinetic measurements of the ^{213}Bi activity were performed to estimate the entrapment of ^{213}Bi, the last γ-emitting daughter in the decay chain, by extrapolation of the monoexponential fit curve of the increasing ^{213}Bi activity to the time point of chromatographic separation.

Liposome immunolabeling

The protocol to immunolabel liposomes has been previously described (18). Briefly, Trastuzumab (5-10 mg/ml, in PBS, pH=8) was purified from Herceptin® (Genentech, South San Francisco, CA) and was reacted with Traut's reagent for 1 hr at room temperature under a nitrogen atmosphere. Then the antibody was purified by SEC in a 10DG column (Biorad, Hercules, CA) eluted with PBS (1mM EDTA, pH=7.4). An average of 5-7 sulfhydril groups per antibody were determined using the Ellman's assay and a protein assay (DC protein assay,

Biorad, CA). Liposomes (7-15 mM lipid) containing maleimide-PE (1 mole% of total lipid) were then incubated with antibody solution (0.5-5 mg/ml) overnight at room temperature under N_2. After completion of conjugation, excess maleimide groups were quenched with β-mercaptoethanol (3:1 molar ratio) for 30 minutes. Immunoliposomes were purified from unreacted antibody and β-mercaptoethanol by size exclusion chromatography in a 4B (Sigma-Aldrich) packed 1x10 cm column, eluted with PBS. A protein assay was used to quantify the concentration of antibodies in the liposome suspension. Lipid concentration was determined by the fluorescence intensity of rhodamine-PE containing liposomes (0.5-1 mole% of total lipid). The average number of antibodies per liposome was estimated using the assumption that for 750 nm diameter liposomes, and 70$Å^2$ head group surface area per lipid (26), a liposome would consist of an average of 5 million lipid molecules.

For control measurements, Trastuzumab was also directly radiolabeled with ^{225}Ac. This preparation protocol is published elsewhere (27).

Immunoreactivity

The immunoreactivity of all liposomal structures and radiolabeled Trastuzumab was determined by incubating the radiolabeled forms with SKOV3 cells. Cells were washed twice with ice-cold PBS and blocked by incubation on ice with 2% BSA. Then, radiolabeled antibody (2.6 ng) in 1% HSA, vesicles and liposomes (1.0-1.9 μg or 100-190 μg total lipid) were added to 10^7 cells, and incubated on ice for 30 min. Cells were then washed twice with ice-cold PBS and centrifuged. Twenty-four hours after centrifugation, the supernatants and pellet were counted by scintigraphy (Beckman-Coulter, Fullerton, CA).

Cell culture and Tumor inoculation

Stock T-flask cultures of the human ovarian carcinoma cell line SKOV3-NMP2 (14) were propagated at 37^{o}C, in 5% CO_2 in RPMI 1640 media supplemented with 10% fetal calf serum (Sigma-Aldrich), 100 units/ml penicillin, and 100 μg/ml streptomycin. Cell concentration was determined by counting trypsinized cells with a hemocytometer. Tumor inoculation was prepared from a single cell suspension in DME medium (Dulbecco's Modified Eagle's Medium). Each 4-6 week old female Balb/c nude mouse (Taconic, Germantown, NY) received 0.15-0.20 ml inoculum of $5x10^6$ cells administered by intraperitoneal injection.

Mice were housed in filter top cages and provided with sterile food and water. Animals were maintained according to the regulations of the Research Animal Resource Center (RARC) at Memorial Sloan-Kettering Cancer Center (MSKCC), and animal protocols were approved by the Institutional Animal Care and Use Committee (IACUC).

Cell Binding and internalization of liposomes and radiolabeled antibody

To quantitate cell binding and internalization of liposomes and radiolabeled antibody, harvested SKOV3 cells were washed twice with ice-cold media (RPMI 1640/ 10% FBS/ 2% BSA) and then resuspended in cold media (as above) at a density of 10^6 cells/ml. Radiolabeled liposomes (0.1 – 1.8 μM lipid, final concentration) or antibody (25 ng) were added to 3.5 ml of cell suspension and two 200 μl samples were immediately taken and processed as described below. The cells were then placed in a humidified, 37^{o}C incubator with 5% CO_2, where they were periodically swirled and sampled at 0.5, 1, 2, 4, and 24 hrs. The cells were washed three times with 2 ml of ice-cold PBS, and then 1 ml of an acidic striping buffer (50 mM glycine, 150 mM NaCl, pH=2.8) was added for 10 minutes at room temperature to eliminate the charge-specific binding of membrane bound conjugates and to remove the surface bound immunoliposomes or antibodies. After centrifugation, the supernatant and pellet were allowed to reach equilibrium (for 20 hours),

and they were then counted to determine the percentages of membrane-bound and internalized counts.

Flow cytometry

Flow cytometry was used to determine the specific binding of liposomes to SKOV3 cells. The liposomal membrane was labeled with the fluorescent lipid rhodamine-PE (excitation: 550 nm; emission: 590 nm). Harvested cells (ovarian cancer SKOV3 cells and fibroblast AL67 cells) were washed three times with ice-cold buffer (PBS/ 0.5% BSA/ 0.02% NaN_3) and then resuspended at a density of $5.6x10^6$ cells/ml. 10^6 cells were incubated on ice with liposomes for 25 minutes (3.3 mM final lipid concentration), then washed three times and finally resuspended at a density of $2.5x10^6$ cells/ml. To determine the extend of specific binding of immunoliposomes to the HER2/neu antigen receptor, cells were also preincubated with Trastuzumab at 5μg of antibody per one million cells for 25 minutes on ice. Cells were then washed twice with ice-cold buffer and incubated with liposomes as above. Fluorescence counting of cell suspensions was measured using a Beckman-Coulter Cytonics FC500 flow cytometer (Fullerton, CA), and analyzed with the software FlowJo (Tree Star, Inc., Ashland, OR).

Excised organ quantitation

Six- to eight- week old female Balb/c nude mice were injected with liposomes (small vesicles, large shells, multivesicular liposomes) (0.2 ml suspension, 0.6-2.7 μmole total lipid) with entrapped ^{225}Ac (0.07-0.2 μCi), and with ^{225}Ac-labeled trastuzumab (2.5 μg; 0.09 μCi) and were sacrificed at four and twenty-four hours post-injection by CO_2 intoxication for dissection. Three to five mice were used per data point. Blood was collected via cardiac puncture. Organs (liver, spleen, and kidneys) and tumor were washed in PBS and weighed. The samples were then counted for the 440 keV ^{213}Bi photons in a γ-counter (Cobra, Packard Instrument Co., Inc.). The

equilibrium values of ^{213}Bi activity were used to estimate accumulation of ^{225}Ac in the blood, organs and tumor. The kinetic profile of ^{213}Bi activity was used to estimate accumulation of ^{213}Bi at the time of animal killing by extrapolation of the monoexponential fit curve of the increasing ^{213}Bi activity to the time point of sacrifice. Results were expressed as percentage of total radioactivity injected in each organ divided by the organ mass (%ID/g).

Whole body clearance in tumor free mice

Multivesicular liposomes, large shell liposomes, and small vesicles with entrapped ^{225}Ac, and also DOTA-^{225}Ac were administered IP in tumor-free 6-8 week old female Balb/c mice (Taconic, Germantown, NY). The whole body clearance was evaluated for up to 24 h post injection by measuring the activity of the γ-photon emissions of the decay of ^{221}Fr and ^{213}Bi by placing the animals at a constant position in front of a 5'' NaI crystal detector connected to a Canberra (Series 20) multichannel analyzer. Five animals were used per injectate. To correct for variations in sensitivity, the counts from a known radioactivity sample were recorded: a 20 ml glass scintillation vial containing the radioactivity of one (corresponding) administered dose, diluted in 20 ml total volume, was used.

Results

Liposome Characterization

Liposome size distributions were determined by DLS. The measured average large liposome size for MUVELs was 758 ± 287 nm. The phospholipid-cholesterol combinations chosen for the small encapsulated vesicles and the large liposome shells were those that resulted in: (1) the lowest release of contents by the small vesicles after annealing at 40^{o}C (this step is required for the hydration of the membranes of the large shell liposomes that contain encapsulated small vesicles), (2) the greatest passive entrapment efficacy, of total activity used, by the large liposome shells, and (3) the minimum fraction of fusion between lipids of small vesicles and large liposomes. Stability of the various membrane structures over time was evaluated by entrapment of a fluorophore (calcein) and assessment of content retention. Content retention by all structures was high for a period of 30 days (data not shown).

Retention of ^{225}Ac by the Liposomal Structures

For 30 days, more than 95% of the encapsulated ^{225}Ac activity was retained by the multivesicular liposomes (black triangles) and small vesicles (black circles) (Figure 2). The large shell liposomes with encapsulated ^{225}Ac directly within their aqueous compartment retained stably only about 70% of the total activity (white circles) (Figure 2)

Retention of ^{213}Bi by the Liposomal Structures

Retention of ^{213}Bi, the last α-emitting daughter of ^{225}Ac, was then evaluated (Figure 3). Multivesicular liposomes (black triangles) and large shell liposomes (white circles) stably retained approximately 18% of ^{213}Bi (32% of the theoretical maximum)(13). Both large liposome structures exhibited almost identical ^{213}Bi retention profiles suggesting that the particular composition of the (external) liposomal membrane does not promote radionuclide localization as opposed to the lipid composition chosen in our first studies (13). However, as shown above

(Figure 2), large shell liposomes failed to adequately retain the parent ^{225}Ac. Also, consistent with our previous theoretical predictions, is the significantly low extent of ^{213}Bi retention (black circles) by small vesicles which have sizes comparable to the recoil range of the α-emitting daughters (28).

Liposome and Antibody Radiolabeling and Quality Control

More than 95% of ^{225}Ac was chelated to the DOTA derivative. The efficiency of conjugation to antibody was low with radiochemical yield 3% (of the total activity applied) and resulted in radiolabeled antibodies with low specific activity, 0.038 μCi/μg.

The maximum encapsulation efficiency of ^{225}Ac by the liposomal structures using passive entrapment did not exceed 10% of the total initial activity, and resulted in one ^{225}Ac nuclide in approximately every eight-to-nine MUVELs.

Immunoreactivity is expressed as per construct and per Trastuzumab molecule. The Her2/neu cell-surface density of 1-3 x 10^5 for these cells was used (29), and approximately one hundred Trastuzumab molecules per cell were mixed. For liposomal structures, two ratios were tested: (a) one hundred liposomes per cell, and (b) one liposome per cell (assuming an estimate of 100 conjugated Trastuzumab antibodies per liposome). The antigen binding activity of liposomes was similar for both ratios tested: 4.40 ± 0.89 % of immunolabeled multivesicular liposomes, and 1.83 ± 0.52 % of immunolabeled large shells were bound to cells. Small plain vesicles bound non-specifically at the extent of 0.75 ± 0.02 %. The immunoreactivity of radiolabeled Trastuzumab was 65.74 ± 7.51 %.

Liposome immunolabelling

The conjugation reaction resulted in 100-500 antibodies per liposome. Leakage of entrapped radioactive or fluorescent (calcein) contents due to conjugation, was not detected (data not shown).

Cell Binding and Internalization

To quantitatively determine binding, and intracellular retention of liposomal contents, all liposomal structures with entrapped ^{225}Ac, and also the radiolabeled antibody, were incubated at 37^{o}C with SKOV3 cell suspensions for different times. Figure 4 shows the fraction of the total initial-activity that became cell-associated (closed symbols), and the fraction of cell-internalized activity (open symbols) for all cell-bound structures. All structures exhibited increase in cell-associated radioactivity with time, followed by gradual saturation of receptor internalization. The total cell-associated radioactivity at different times after start of incubation was compared to that immediately after the start of incubation (t=0). After 4 hours, the relative increases were a 2-, 7- and 135-fold for large shell immunoliposomes (squares), MUVELs (circles), and radiolabeled antibody (triangles), respectively. At 4 hours, the fraction of total cell-associated activity for non-immunolabeled MUVELS, large shells and small vesicles was 0.47%, 0.61% and 0.16% of the total added radioactivity, respectively (data not shown). After 4 h of incubation, the fraction of total cell-associated activity (^{225}Ac) delivered by specifically targeted multivesicular immunoliposomes (2.5 ± 0.5 %) was 3.8 times greater than the fraction of total associated radioactivity delivered by large shell immunoliposomes (0.7 ± 0.1 %), probably due to the less stable retention of the parent nuclide by the large shell liposomes (Figure 2). Also, immunoliposomes internalized to a greater extent than the antibody: 83% of the activity of bound multivesicular immunoliposomes, and 70% of the activity of large shell immunoliposomes were internalized (4 h incubation) as opposed to only 23% of bound antibody. Cell uptake kinetics were significantly slower for all liposome structures compared to the radiolabeled antibody.

Flow cytometry was also used to evaluate the specific binding of immunoliposomes (by monitoring the fluorescently labeled membranes) to cell suspensions expressing, or not, the HER2/neu receptor (SKOV3 and AL67 fibroblast cell lines, respectively) (Figure 5). Significant shift in fluorescence counts (one log unit) that signifies enhanced binding of liposomes to cells was detected only when immunoliposomes were incubated with SKOV3 cells with unblocked HER2/neu receptors (Figure 5A, thick line). Neither specific nor non-specific binding of liposomes to AL67 cells was detected.

Whole body retention by tumor free mice

The whole body clearance of ^{221}Fr and ^{213}Bi in tumor free mice was low when radionuclides were administered within liposomal structures. Twenty-four hours post-administration, at least 81 % of the initial whole body activity was retained. On the contrary, rapid whole body clearance was observed after administration of ^{225}Ac-DOTA: Four hours post injection more than 90% of the total injected activity of ^{213}Bi and more than 96 % of ^{221}Fr was cleared from the body. No preferential clearance between the two radioactive daughters was observed when liposomes were used. At all time points, the ratios of the activity of ^{221}Fr to the activity of ^{213}Bi did not significantly deviate from the value obtained for the glass vial 'phantom' that contained the radioisotopes at equilibrium conditions.

Biodistributions of Liposomal Structures in Tumor Bearing Mice

Biodistributions of all liposomal structures and the free radiolabeled antibody were determined in tumor bearing mice. Fourteen days after inoculation, a tumor pattern was formed, that consisted of nodules on the ventral side of the spleen. Smaller nodules (~ 1mm in diameter) were frequently observed within the mesentery. The mean weight of removable tumor nodules was 0.3 ± 0.2 g (n=29, total number of animals). The normal organ accumulation of liposomes

reached steady state levels 8 h after administration, and the tumor uptake was (almost by 6-times) faster for Trastuzumab-labeled liposomes against HER2/neu overexpressing SKOV3 tumors compared to liposomes without conjugated antibodies.

The biodistribution of ^{225}Ac delivered by immunolabeled MUVELs was compared to the following structures (constructs) containing ^{225}Ac: (a) immunolabeled large shell liposomes with encapsulated ^{225}Ac in their aqueous phase, (b) small vesicles with encapsulated ^{225}Ac in their aqueous phase and without conjugated antibodies on their surface, and (c) Trastuzumab-antibody conjugated to ^{225}Ac. The radioactivity distribution is represented as the tissue-to-kidney activity concentration ratio, since kidneys are the dose-limiting organ for ^{225}Ac due to ^{213}Bi selective accumulation. Among the different liposomal structures that were used to specifically deliver ^{225}Ac to cancer cells *in vivo*, multivesicular immunoliposomes showed the highest tumor-to-kidney uptake at both time points studied (Figure 6A). Four hours after administration the tumor-to-kidney ratio for multivesicular immunoliposomes was 6.9 ± 2.1 (black bars) and twenty-four hours later it further increased to 9.8 ± 4.4 (white bars). MUVELs exhibited significantly slower kinetics of tumor uptake compared to radiolabeled trastuzumab. The antibody demonstrated high initial tumor ratio of 15.5 ± 3.3 at 4 h, which decreased to 11.7 ± 0.6 24 h later. At that time point, the measured ^{225}Ac ratios at the tumor delivered by MUVELs and the radiolabeled antibody were not significantly different. Kidney and blood uptake of ^{225}Ac was low for all structures at the time intervals tested. The accumulation of radioactivity to the spleen at a significant extent, and to the liver, at a lesser degree, is consistent with reported values of liposome localization and probably does not reflect antibody targeting.

The biodistributions of ^{213}Bi, the last α-emitting daughter, was also evaluated for all constructs. Figure 6B shows the radioactivity distribution of ^{213}Bi as the tissue-to-kidney activity concentration ratio. At both time points (4 and 24 hours after administration), multivesicular

immunoliposomes exhibited the highest tumor-to-kidney ratios among all other liposomal structures and the radiolabeled antibody.

DISCUSSION

Alpha-particle emitters are considered potent radiotherapeutics for the treatment of micrometastatic disease due to their high LET and the short range of α-particles that is comparable to the size of micrometastases.

Actinium-225 is a highly promising α-particle atomic nanogenerator due to the four α-particles emitted per decay (Figure 1A). However, ^{225}Ac can be highly toxic due to the three resulting α-particle emitting daughters. The α-emitting daughters are not retained by molecular radioconjugates (antibodies or polymers), because the energy of the bond between parent nuclide and chelate is smaller than the daughter's recoil energy. Upon decay of ^{225}Ac, the newly formed α-emitting daughter, ^{221}Fr, recoils away from the original radioconjugate. To retain the radioactive daughters at the target site, we have developed multivesicular liposomes (MUVELs) as an alternative delivery carrier. In MUVELs, ^{225}Ac is encapsulated into small vesicles that are contained within large liposomes. We designed this structure to increase the probability that the end point of the daughter's recoil trajectory (80-100 nm) will lay within the internal part of the liposome (~ 750 nm diameter) by 'forcing' ^{225}Ac to localize closer to the liposomal core. If the nuclide decay occurs at the liposomal membrane, there is almost 50% chance the newly formed radioactive daughter will be ejected out of the liposomes, and then the location of the subsequently emitted α-particle will not be controlled.

In this study we demonstrated that MUVELs result in minimal leakage of ^{225}Ac and in significant retention of the α-emitting daughters *in vitro*. When ^{225}Ac is delivered by MUVELs we have control of 2.6 out of 4 α-particles emitted per ^{225}Ac decay.

MUVELs were further engineered to specifically target human ovarian carcinoma cells (SKOV3). *In vitro*, the Trastuzumab-labeled MUVELs demonstrated greater specific cell binding compared to non targeted liposomes, but immunoliposomes showed lower immunoreactivity compared to the free radiolabeled antibody. The relatively lower immunoreactivity of liposomes could be due to the relatively large size of liposomes that may interfere with the cellular surface architecture (the extracellular matrix). Neighboring grafted PEG-chains on the liposome surface are not expected to present steric hindrance, because the targeting antibodies were conjugated to the free-ends of surface-grafted PEG-chains of the same length (30). In addition, slower kinetics of cell uptake for the immunoliposomes compared to free antibody were observed *in vitro*. The slower kinetics could be justified by the different diffusivities of each structure studied. Measured diffusion coefficients of free IgG's are of the order of 10^{-7} cm^2/sec in water at 20^oC (31). At the same conditions, the calculated values for large liposomes (using the Stokes-Einstein equation for spherical objects) are 2 orders of magnitude lower (10^{-9} cm^2/sec).

The lipid-based carriers were also evaluated *in vivo*. Antibody-labeled MUVELs containing ^{225}Ac were administered intraperitoneally (IP) in animals bearing small-size tumors. These tumors resemble disseminated micrometastatic disease in the peritoneal cavity, and are the optimal target for α-particle therapy. This particular disease topology is common among patients with advanced gynecological and gastrointestinal cancers, and IP administration can provide direct access to the intraperitoneal micrometastases. In ^{225}Ac-radioimmunotherapy, renal toxicity can become a major dose constraint due to localization of escaped radioactive daughters (e.g. ^{213}Bi) in the kidneys (32). For peritoneally disseminated disease, large liposomes may provide an alternative delivery vehicle by retaining most of the radioactive daughters at the site of the carrier.

In vivo, the tumor uptake kinetics of ^{225}Ac mediated by MUVELs were significanlty slower than the accumulation observed for the radiolabeled antibody. Tumor uptake was comparable for the two constructs only 24 hours after administration. Due to the increased residence time of MUVELs in the IP cavity, a further increase with time of ^{225}Ac tumor accumulation mediated by MUVELs should be expected. In liposome administered animals, the measured whole body activities are greater than the sum of activities from the excised organs, suggesting prolonged retention (of $\approx$ 50%) of the injected liposome-associated activity in the peritoneal cavity (free ^{225}Ac-DOTA is rapidly cleared from the body). Direct sampling and characterization of peritoneal fluid was not performed. The slower peritoneal clearance of liposomes compared to the fast clearance of radiolabeled antibodies (33) could be a potential advantage for immunolabeled MUVELs with entrapped long-lived α-particle emitters decaying to multiple α-particle emitting daughters in localized treatments. Liposomes would, therefore, provide a longer available time to diffuse within the peritoneal cavity, allowing for greater tumor uptake over a prolonged time-peroid.

Comparison between the ratios of ^{213}Bi- to ^{225}Ac- activities at the tumor site for immunolabeled MUVELs and radiolabeled antibodies have been obtained (Figure 6C). Although MUVELs retained 18% of the ^{213}Bi daughter, this did not translate to a significant improvement in the tumor to kidney ^{213}Bi activity concentration ratio at 4 and 24 h after injection. This can be explained by the higher localization of MUVELs to liver and spleen relative to the radiolabeled antibody. Tumor localization of MUVELs will lead to MUVEL internalization by targeted tumor cells and therefore enhanced retention of Bi-213 at the tumor site. Localization to spleen and liver, on the other hand is likely to lead to MUVEL catabolism and release of free ^{225}Ac and, therefore, free ^{213}Bi. A reduction in spleen and liver MUVEL localization, by pre-injection of non-specific, non-radioactive liposomes would shift the biodistribution towards the

tumor leading to enhanced retention of ^{213}Bi at the tumor site relative to ^{225}Ac-labeled antibody. Furthermore, since the relevant quantity regarding tumor control is the time-integrated delivery of alpha-particles over the effective lifetime of ^{225}Ac, the ratios at 4 and 24 hrs are not necessarily indicative of therapeutic effect relative to renal toxicity.

In figure 6c, values closer to unity, signify that less ^{213}Bi has escaped from the tumor or the delivery/targeting construct bound to the tumor. Enhanced retention of α-particle emitting daughters by the targeted cancer cells will increase the killing efficacy of ^{225}Ac. For MUVELs the ratio does not significantly change over time and is closer to 0.89 for both time points. This value agrees with the *in vitro* cell-binding studies that showed high internalization fraction (83%) for cell-bound MUVELs and the significant retention of ^{213}Bi by MUVELs. For the radiolabeled antibody, the ^{213}Bi activity relative to the ^{225}Ac activity delivered at the tumor increases with time from 0.66 at four hours to 0.76 at twenty-four hours post-administration. This result agrees with the fast binding kinetics of the radiolabeled antibody combined with fast clearance of the antibody from the peritoneal cavity (33). Since α-particles originating on the cell surface have only an estimated 30% probability of traversing the cell nucleus (34), the high internalization extent of cell-bound MUVELs is a positive characteristic of this approach.

Finally, the radiation dose that can actually be delivered at the tumor sites would be substantially increased by MUVELs, especially for cancer cells that express relatively low levels of the targeted surface antigens (35). Radiolabeled antibodies with ^{225}Ac have generally low specific activity (0.038 mCi/mg in this study) that corresponds to one conjugated ^{225}Ac atom per 2,300 antibodies. With the current entrapment strategy, for MUVELs, two passive entrapment steps are required (each with a maximum of 10% encapsulation efficiency). Thus, for 1mCi ^{225}Ac initial activity, and 1% actinium overall entrapment efficacy, we can achieve one

encapsulated ^{225}Ac nuclide per 8.7 MUVELs (assuming 4x10^{12} liposomes with a mean diameter of 750nm). Increase of the initial activity to 10 mCi ^{225}Ac should result in one actinium nuclide per MUVEL and two actinium nuclides in every 8 MUVELs. Thus, higher effective delivered dose at the tumor can, in principle, be reached using MUVELs. Current work is focused on increasing the encapsulated ^{225}Ac activity within small vesicles using active (ionophore-driven) loading. Further structural optimization of MUVELs is also required, to further increase the retention of radioactive daughters at the liposome sites and to minimize renal accumulation of free radioactive daughters.

The *in vivo* studies showed significant spleen uptake of MUVELs that may potentially affect the dosimetry and therapeutic potential of this approach. The impact of such localization on toxicity will require MTD studies. It is important to note that the relatively short range of α-particles (80-100 μm, or approximately 5 cell diameters), and their microscopic distribution in the spleen may mitigate potential toxicity. There is evidence that liposomes are taken up by splenic macrophages rather than parenchymal splenic cells (36). Similarly, regarding the liver uptake, liposome accumulation may be attributed to opsonin-mediated uptake by Kupffer cells at the endothelial hepatic sites, without reported penetration into the parenchymal region. Also, as noted above, the administration of non-specific, non-radioactive liposomes prior to the MUVELs could reduce uptake by the reticuloendothelial system (RES) and increase MUVEL localization to the target site. Such an approach to reduce RES uptake has been previously demonstrated ().

Intraperitoneal micrometastatic disease constitutes a treatment challenge. In this work, the ovarian carcinoma model was selected as a proof of principle for delivery of the α-particle nanogenerator ^{225}Ac to disseminated intraperitoneal micrometastases using MUVELs and

locoregional administration. Our findings suggest that radioimmunolabeled MUVELs could potentially reduce the toxicity associated with the untargeted radioactive daughter emissions of ^{225}Ac while increasing delivery of α-particle emissions per targeted cells, providing a promising therapeutic modality for disseminated micrometastatic disease. Additional optimization of these structures is necessary.

References

1. Couturier, O., Supiot, O., Degraef-Mougin, M., Faivre-Chauvet, A., Carlier, T., Chatal, J. F., and Cherel, M. Cancer radioimmunotherapy with alpha-emitting nuclides. Eur J Nucl Med Imaging, *32:* 601-614, 2005.
2. Humm, J. L. A microdosimetric model of astatine-211 labeled antibodies for radioimmunotherapy. Int J Radiat Oncol Biol Phys, *13:* 1767-1773, 1987.
3. Humm, J. L. and Chin, L. M. A model of cell inactivation by alpha-particle internal emitters. Radiat Res, *134:* 143-150, 1993.
4. Macklis, R. M., Kinsey, B. M., Kassis, A. I., Ferrara, J. L., Archer, R. W., Hines, J. J., Coleman, C. N., Adelstein, S. J., and Burakoff, S. J. Radioimmunotherapy with alpha-particle-emitting immunoconjugates. Science, *240:* 1024-1026, 1988.
5. McDevitt, M. R., Ma, D., Lai, L. T., Simon, J., Borchardt, P., Frank, R. K., Wu, K., Pellegrini, V., Curcio, M. J., Miederer, M., Bander, N. H., and Scheinberg, D. A. Tumor therapy with targeted atomic nanogenerators. Science, *294:* 1537-1540, 2001.
6. Kennel, S. J., Brechbiel, M. W., Milenic, D. E., Schlom, J., and Mirzadeh, S. Actinium-225 conjugates of MAb CC49 and humanized delta CH2CC49. Cancer Biother Radiopharm, *17:* 219-231, 2002.
7. Kennel, S. J., Chappell, L. L., Dadachova, K., Brechbiel, M. W., Lankford, T. K., Davis, I. A., Stabin, M., and Mirzadeh, S. Evaluation of Ac-225 for vascular targeted radioimmunotherapy of lung tumors. Cancer Biother Biopharm, *15:* 235-244, 2000.
8. Emfietzoglou, D., Kostarelos, K., and Sgouros, G. An analytic dosimetry study for the use of radionuclide-liposome conjugates in internal radiotherapy. J. Nucl. Med, *42:* 499-504, 2001.
9. Emfietzoglou, D., Kostarelos, K., Papakostas, A., Yang, W. H., Ballangrud, A., Song, H., and Sgouros, G. Liposome-mediated radiotherapeutics within avascular tumor spheroids: comparative dosimetry study for various radionuclides, liposome systems, and a targeting antibody. J Nucl Med, *46:* 89-97, 2005.
10. Kostarelos, K., Emfietzoglou, D., Papakostas, A., W.H., Y., Ballangrud, A. M., and Sgouros, G. Engineering lipid vesicles of enhanced intratumoral transport capabilities: correlating liposome characteristics with penetration into human prostate tumor spheroids. J Liposome Res, *15:* 15-27, 2005.
11. Kostarelos, K. and Empfietzoglou, D. Tissue dosimetry of liposome-radionuclide complexes for internal radiotherapy: toward liposome-targeted therapeutic radiopharmaceuticals. Anticancer Res, *20*, 2000.
12. Kostarelos, K., Empfietzoglou, D., Papakostas, A., Yang, W.-H., Ballangrud, A., and Sgouros, G. Binding and interstitial penetration of liposomes within avascular tumor spheroids. Int J Cancer, *112:* 713-721, 2004.
13. Sofou, S., Thomas, J. L., Lin, H.-Y., McDevitt, M. R., Scheinberg, D. A., and Sgouros, G. Engineered liposomes for potential α-particle therapy of metastatic cancer. J Nucl Med, *45:* 253-260, 2004.
14. Borchardt, P., Yuan, R., Miederer, M., McDevitt, M., and Scheinberg, D. Targeted actinium-225 in vivo generators for therapy of ovarian cancer. Cancer Res, *63:* 5084, 2003.
15. Buijs, W. C. A. M., Tibben, J. G., Boerman, O. C., Molthoff, C. F. M., Massuger, L. F. A. G., Koenders, E. B., Schijf, C. P. T., Siegel, J. A., and Corstens, F. H. M. Dosimetric analysis of chimeric monoclonal antibody cMOv18 IgG in ovarian

carcinoma patients after intraperitoneal and intravenous administration. Eur J Nucl Med, *25:* 1552-1561, 1998.
16. Markman, M. Role of intraperitoneal chemotherapy in the front-line setting. J Clin Oncol, *21:* 145s-148s, 2003.
17. Li, C.-Y., Shan, S., Huang, Q., Braun, R. D., Lanzen, J., Hu, K., Lin, P., and Dewhirst, M. W. Initial Stages of Tumor Cell-Induced Angiogenesis: Evaluation Via Skin Window Chambers in Rodent Models. J Natl Cancer Inst, *92:* 143-147, 2000.
18. Kirpotin, D. B., Park, J. W., Hong, S. K., Zalipsky, S., Li, W.-L., Carter, P., Benz, C. C., and Papahadjopoulos, D. Sterically stabilized anti-HER2 immunoliposomes: design and targeting to human breast cancer cells *in vitro*. Biochemistry, *36:* 66-75, 1997.
19. Sapra, P. and Allen, T. M. Ligand-targeted liposomal anticancer drugs. Prog Lipid Res, *42:* 439-462, 2003.
20. Sadzuka, Y., Hirota, S., and Sonobe, T. Intraperitoneal administration of doxorubicin encapsulating liposomes against peritoneal dissemination. Toxicol Letters, *116:* 51-59, 2000.
21. Verschraegen, C., Kumagai, S., Davidson, R., Feig, B., Mansfield, P., Lee, S., Maclean, D., Hu, W., Khokhar, A., and Siddik, Z. Phase I clinical and pharmacological study of intraperitoneal cis-bis-neodecanoato(trans- R, R-1, 2-diaminocyclohexane)-platinum II entrapped in multilamellar liposome vesicles. J Cancer Res Clin Oncol, *129:* 549-555, 2003.
22. Sofou, S., Scheinberg, D. A., and Sgouros, G. Novel liposomes with unique internal structure. manuscript.
23. Stensrud, G., Redford, K., Smistad, G., and Karlsen, J. Effects of gamma irradiation on solid and lyophilised phospholipids. Rad Phys Chem, *56:* 611-622, 1999.
24. Provencher, S. W. A constrained regularization method for inverting data represented by linear algebraic or integral equations. Comput Phys Commun, *27:* 213-227, 1982.
25. Teraoka, I. Polymer Solutions: An Introduction to Physical Properties, 1st edition edition, p. 188-191. New York, NY: John Wiley & Sons, 2002.
26. Lasic, D. D. Liposomes from Physics to Applications, p. 555. Amsterdam: Elsevier, 1993.
27. Jurcic, J. G., Larson, S. M., Sgouros, G., McDevitt, M. R., Finn, R. D., Divgi, C. R., Ballangrud, A. M., Hamacher, K. A., Ma, D. S., Humm, J. L., Brechbiel, M. W., Molinet, R., and Scheinberg, D. A. Targeted alpha-particle immunotherapy for myeloid leukemia. Blood, *100:* 1233-1239, 2002.
28. Ziegler, J. Stopping and range of ions in matter (SRIM96). Yorktown, New York: IBM, 1996.
29. Dean, G. S., Pusztai, L., Xu, F. J., O'Briant, K., DeSombre, K., Conaway, M., Boyer, C. M., Mendelsohn, J., and Bast, R. C. J. Cell surface density of p185c-erbB-2 determines susceptibility to anti-p185c-erbB-2-Ricin A chain (RTA) immunotoxin therapy alone and in combination with anti-p170EGFR-RTA in ovarian cancer cells. Clin Cancer Res, *4:* 2545-2550, 1998.
30. Maruyama, K., Takizawa, T., Yuda, T., Kennel, S. J., Huang, L., and Iwatsuru, M. Targetability of novel immunoliposomes modified with amphipathic poly(ethylene glycol)s conjugated at their distal terminals to monoclonal antibodies. Biochim Biophys Acta, *1234:* 74-80, 1995.
31. Saltzman, W. M., Radomsky, M. L., Whaley, K. J., and Cone, R. A. Antibody diffusion in human cervical mucus. Biophys J, *66:* 508-515, 1994.

32. Jaggi, J. S., Kappel, B. J., McDevitt, M. R., Sgouros, G., Flombaum, C. D., Cabassa, C., and Scheinberg, D. A. Efforts to control the errand products of a targeted in vivo generator. Cancer Res, *65:* 4888-4895, 2005.
33. Palm, S., Enmon, R. M., Matei, C., Kolbert, K. S., Xu, S., Zanzonico, P., Finn, R. D., Koutcher, J. A., Larson, S. M., and Sgouros, G. Pharmacokinetics and biodistribution of 86Y-Trastuzumab for 90Y dosimetry in an ovarian carcinoma model: correlative microPET and MRI. J Nucl Med, *44:* 1148-1155, 2003.
34. Nikula, T. K., McDevitt, M. R., Finn, R. D., Wu, C., Kozak, R. W., Garmestani, K., Brechbiel, M. W., Curcio, M. J., Pippin, C. G., Tiffany-Jones, L., Geerlings, S. M. W., Apostolidis, C., Molinet, R., Geerlings, J. M. W., Gansow, O. A., and Scheinberg, D. A. Alpha-emitting bismuth cyclohexylbenzyl DTPA constructs of recombinant humanized anti-CD33 antibodies: pharmacokinetics, bioactivity, toxicity and chemistry. J. Nucl. Med., *40:* 166-176, 1999.
35. McQuarrie, S. A., Mercer, J. R., Syme, A., Suresh, M. R., and Miller, G. G. Preliminary results of nanopharmaceuticals used in the radiotherapy of ovarian cancer. J Pharmaceut Sci, *7:* 29-34, 2004.
36. Ishida, T., Harashima, H., and Kiwada, H. Liposome clearance. Biosci Reports, *22:* 197-224, 2002.

Captions

Figure 1A.

Simplified ^{225}Ac decay cascade with associated particulate decays and half-lives.

Figure 1B.

Effect of liposome size, and parent nuclide position on the retention of ^{225}Ac daughters by liposomes. The average recoil distance of the radionuclides (^{225}Ac and its daughters) is between 80 to 100 nm (solid line arrows) and is comparable to the size of conventional liposomes. Therefore, daughter retention by liposomes increases with liposome size (shown here as concentric circles of increasing radius). The effect of parent radionuclide position is shown for the smaller liposome size and for ^{225}Ac and ^{221}Fr: the closer the nuclear recoil occurs to the liposomal membrane (e.g. ^{221}Fr) the lower the probability that the newly formed daughter (^{217}At) will be retained by the liposome.

Figure 2.

Fraction of ^{225}Ac retention by multivesicular liposomes (▼), large shell liposomes (○), and small vesicles (●) during 30 d. The error bars correspond to standard deviations of repeated measurements.

Figure 3.

Fraction of ^{213}Bi retention by multivesicular liposomes (▼), large shell liposomes (○), and small vesicles (●) during 30 d. The error bars correspond to standard deviations of repeated measurements.

Figure 4.

Cell binding and internalization of immunolabeled ^{225}Ac-entrapping lipid-structures and ^{225}Ac-conjugated antibody. Closed symbols: fraction of the total initial-activity that became cell-associated. Open symbols: fraction of cell-internalized activity. Triangles: radiolabeled antibody; circles: immunolabeled MUVELs; squares: immunolabeled large shell liposomes. The error bars correspond to standard deviations of repeated measurements.

Figure 5.

Binding of rhodamine-lipid-containing Trastuzumab-labeled liposomes to SKOV3 (A) and AL67 cells (B). Shaded grey: cells; Thin line: cell fluorescence due to immunoliposomes bound to cells that have been pre-incubated with Trastuzumab; Thick line: cell fluorescence due to immunoliposomes bound to cells with unblocked receptors.

Figure 6A.

Uptake of ^{225}Ac in various tissues 4 h (black bars) and 24 h (white bars) after intraperitoneal administration of immunolabeled MUVELs, immunolabeled large shell liposomes, not-immunolabeled small lipid vesicles, and ^{225}Ac-labeled Trastuzumab. The error bars correspond to standard deviations.

Figure 6B.

Uptake of ^{213}Bi in various tissues 4 h (black bars) and 24 h (white bars) after intraperitoneal administration of immunolabeled MUVELs, immunolabeled large shell liposomes, not-immunolabeled small lipid vesicles, and ^{225}Ac-labeled Trastuzumab. The error bars correspond to standard deviations.

Figure 6C.

Ratio of ^{213}Bi to ^{225}Ac activities at the tumors 4 h (black bars) and 24 h (white bars) after intraperitoneal administration of immunolabeled MUVELs with encapsulated ^{225}Ac, and ^{225}Ac-labeled Trastuzumab (n = 3 - 5). The error bars correspond to standard deviations.

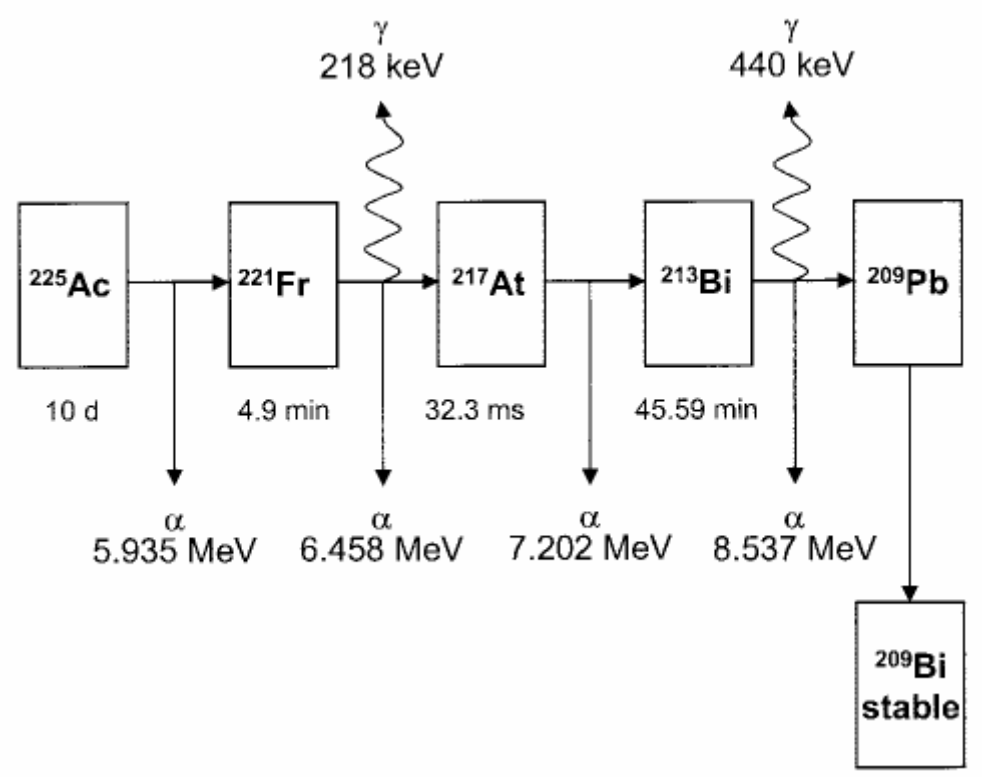
γ
218 keV
γ
440 keV
225Ac
221Fr
217At
213Bi
209Pb
10 d
4.9 min
32.3 ms
45.59 min
α
5.935 MeV
α
6.458 MeV
α
7.202 MeV
α
8.537 MeV
209Bi
stable

Figure 1A

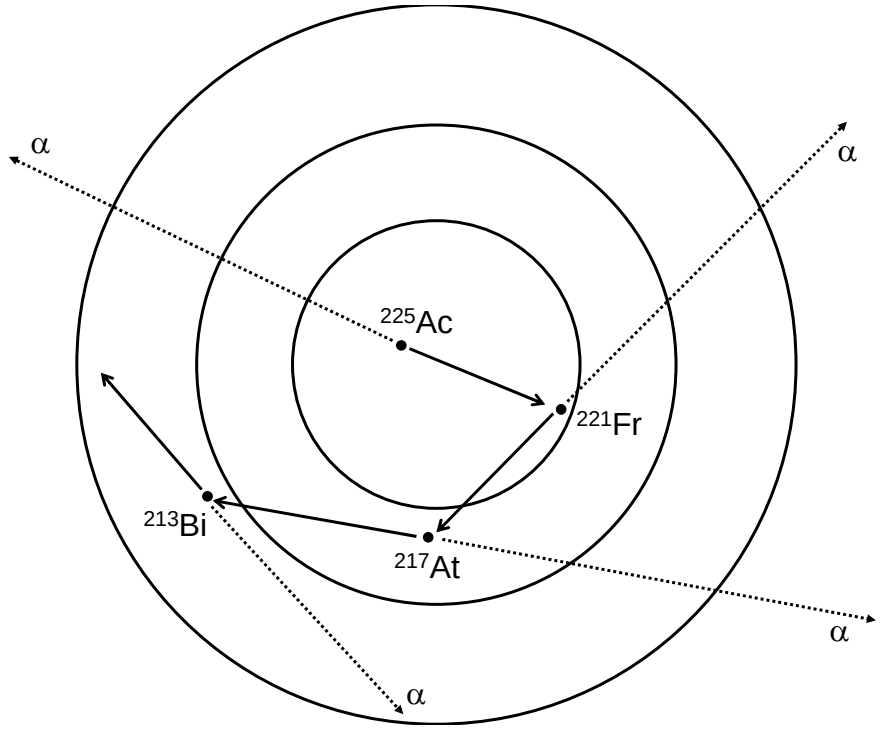

Figure 1B

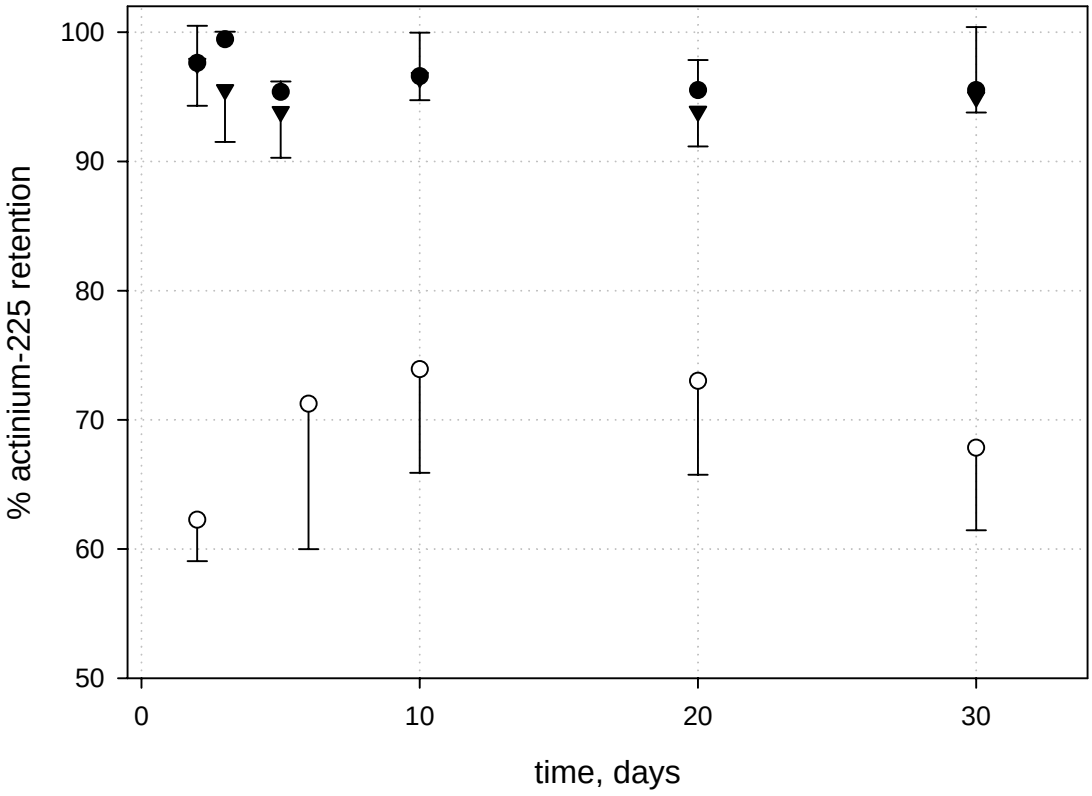

Figure 2

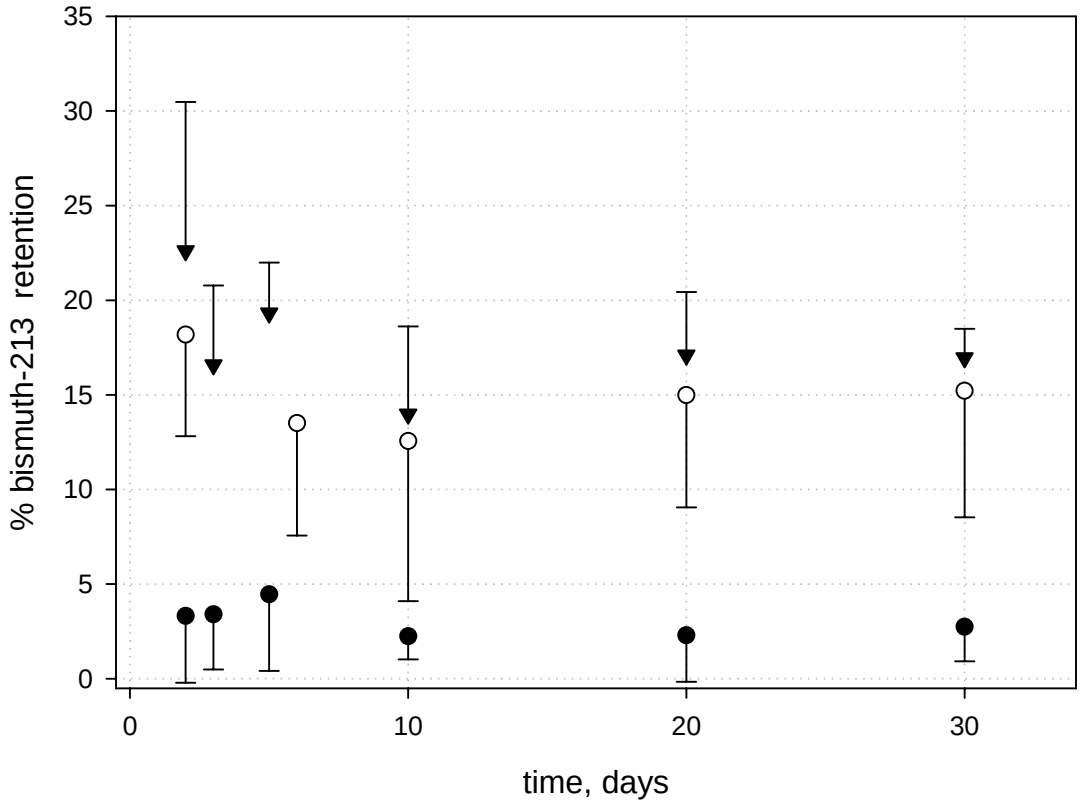

Figure 3

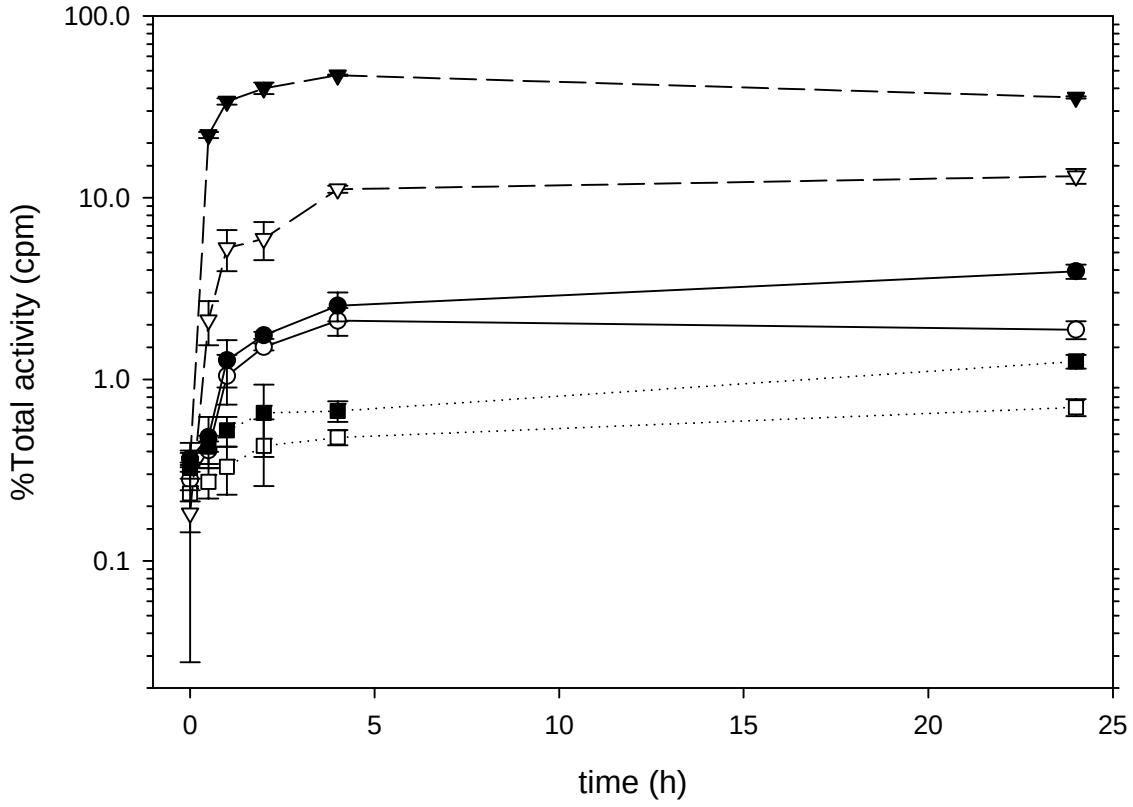

Figure 4

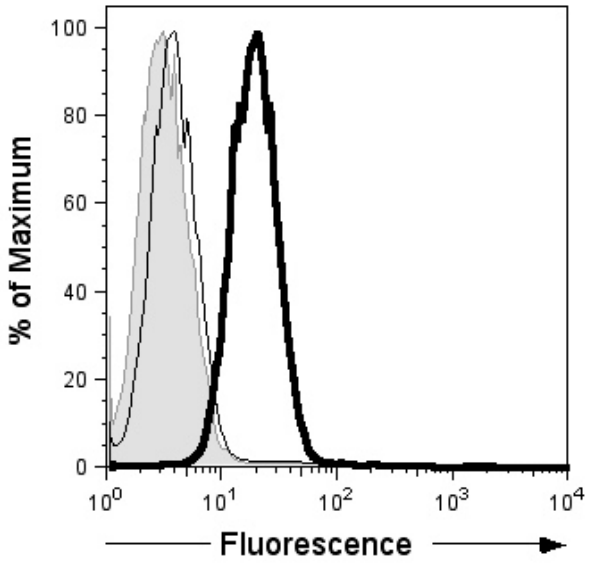

Figure 5A

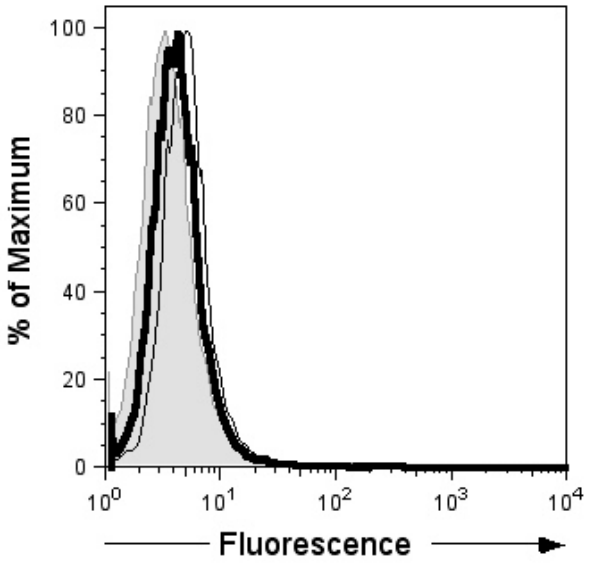

Figure 5B

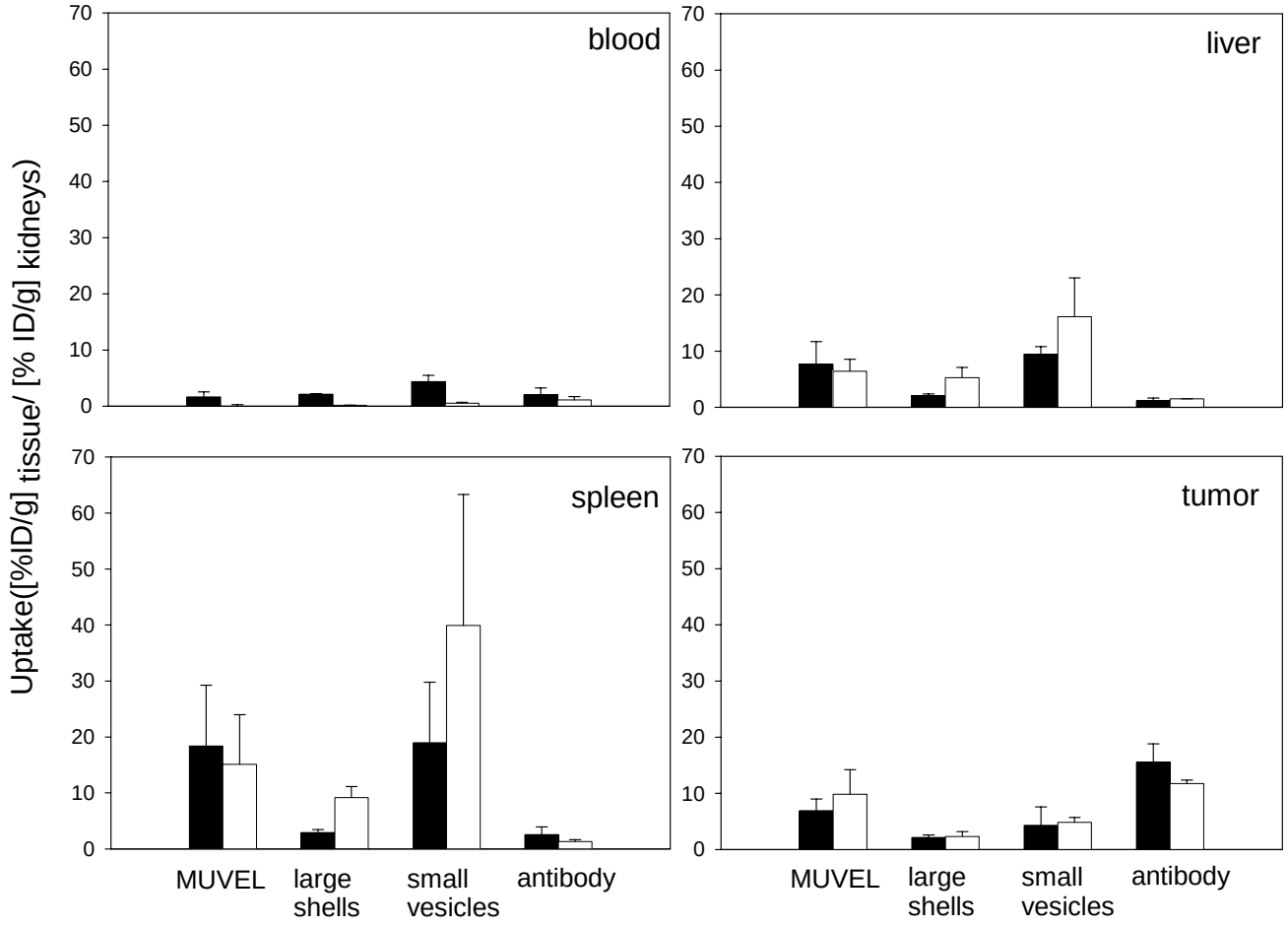
blood
liver
spleen
tumor
Uptake([%ID/g] tissue/ [% ID/g] kidneys)
0
10
20
30
40
50
60
70
MUVEL
large shells
small vesicles
antibody

Figure 6A

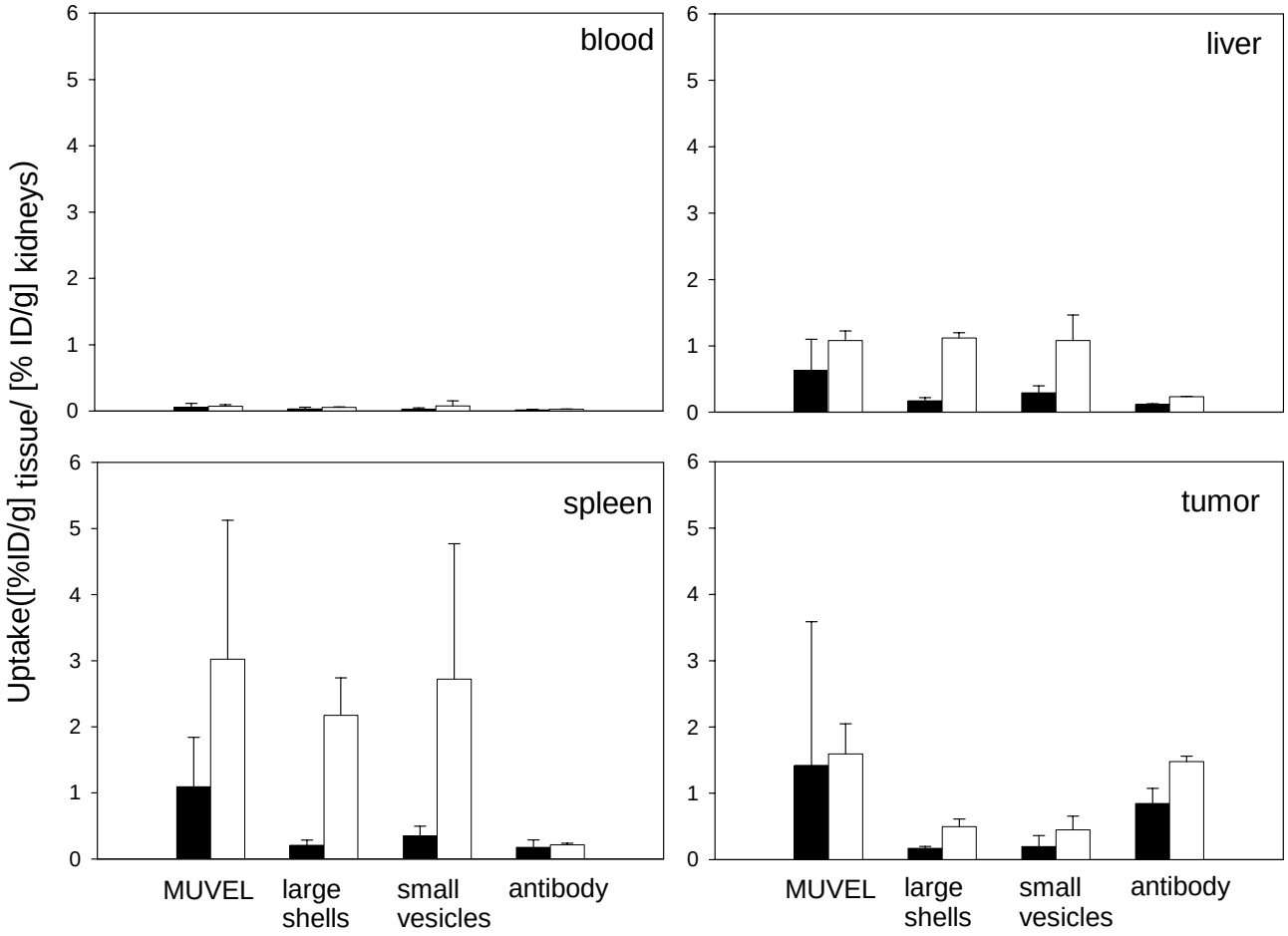
blood
liver
spleen
tumor
Uptake([%ID/g] tissue/ [% ID/g] kidneys)
0
1
2
3
4
5
6
MUVEL
large shells
small vesicles
antibody

Figure 6B

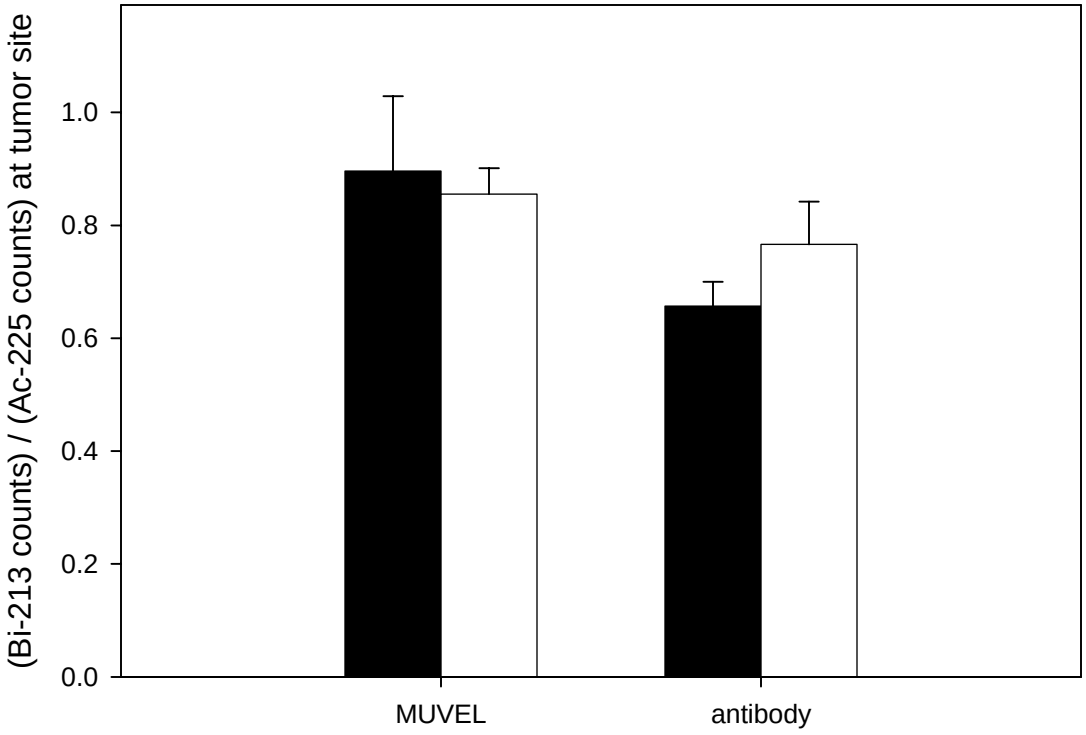
(Bi-213 counts) / (Ac-225 counts) at tumor site
1.0
0.8
0.6
0.4
0.2
0.0
MUVEL
antibody

Figure 6C